

# EPSC2018

## **OPS2 abstracts**

# Cassini Observations of Saturn's Irregular Moons

**Tilman Denk** (1) and Stefano Mottola (2)

(1) Freie Universität Berlin, Germany (Tilman.Denk@gmx.de), (2) DLR Berlin, Germany

## 1. Introduction

With the ISS-NAC camera of the Cassini spacecraft, we obtained photometric lightcurves of 25 irregular moons of Saturn. The goal was to derive basic physical properties of these objects (like rotational periods, shapes, pole-axis orientations, possible global color variations, ...) and to get hints on their formation and evolution. Our campaign marks the first utilization of an interplanetary probe for a systematic photometric survey of irregular moons.

The irregular moons are a class of objects that is very distinct from the inner moons of Saturn. Not only are they more numerous (38 versus 24), but also occupy a much larger volume within the Hill sphere of Saturn. Further, they are quite small: All but Phoebe have sizes in the range ~40 km to ~4 km. Therefore, they significantly contribute to the number, but not to the overall mass of Saturn's moon system (< 0.01%). Widely accepted is the hypothesis that many irregular moons have joint progenitors and form "collisional families". A comprehensive summary on Saturn's irregulars is given by Denk *et al.* (2018) [1]. Earlier summaries on all irregular-moon systems of the giant planets can for example be found in [2], [3], or [4].

## 2. Lightcurves and rotation periods

All 9 known prograde and 16 of the 29 known retrograde Saturnian irregulars were observed over a wide phase-angle range of ~2° to >125°. The average observation distance for Cassini was in the order of  $1.4 \cdot 10^7$  km, corresponding to a spatial resolution below  $80 \text{ km px}^{-1}$ , too low to resolve the irregulars (except Phoebe). The brightness range during the observations was between ~9.5 and ~16.6 mag (Phoebe was occasionally brighter than ~6 mag). All lightcurves but Phoebe's are mainly or exclusively shape-driven and show 2-maxima/2-minima or 3-max/3-min patterns. An exception is a lightcurve of Paaliaq which shows pronounced 4-max/4-min.

The period range of all observed moons is between ~5.5 h and ~76 h (→ Table). The periods of all but

two prograde irregulars are slower than ~13 h, while the periods of all but two retrogrades are faster than ~13 h. The fastest period (Hati) is much slower than the disruption rotation barrier for asteroids (~2.3 h), indicating that Saturn's irregulars may be rubble piles of rather low densities, possibly as low as of comets.

*Table:* Rotational periods of 25 Saturnian irregulars

Moon name	Approx. size [km]	Rotational period [h]
Hati	5	$5.45 \pm 0.04$
Mundilfari	7	$6.74 \pm 0.08$
Loge	5	$6.9 \pm 0.1$ ?
Skoll	5	$7.26 \pm 0.09$ (?)
Suttungr	7	$7.67 \pm 0.02$
Kari	6	$7.70 \pm 0.14$
Bergelmir	5	$8.13 \pm 0.09$
Phoebe	213 [5]	$9.2735 \pm 0.0006$ [6]
Fornjot	6	~9.5 ??
<b>Siarnaq</b>	<b>42</b>	<b><math>10.18785 \pm 0.00005</math></b>
Narvi	7	$10.21 \pm 0.02$
<b>Tarvos</b>	<b>15</b>	<b><math>10.691 \pm 0.001</math></b>
Skathi	8	$11.10 \pm 0.02$
Ymir	19	$11.92220 \pm 0.00002$
Greip	5	$12.75 \pm 0.35$ (?)
Hyrrokkin	8	$12.76 \pm 0.03$
<b>Ijiraq</b>	<b>13</b>	<b><math>13.03 \pm 0.14</math></b>
<b>Albiorix</b>	<b>33</b>	<b><math>13.33 \pm 0.03</math></b>
Bestla	7	$14.6238 \pm 0.0001$
<b>Bebhionn</b>	<b>6</b>	<b><math>16.33 \pm 0.03</math></b>
<b>Paaliaq</b>	<b>25</b>	<b><math>18.79 \pm 0.09</math></b>
<b>Kiviuq</b>	<b>17</b>	<b><math>21.97 \pm 0.16</math></b>
<b>Erriapus</b>	<b>10</b>	<b><math>28.15 \pm 0.25</math></b>
Thrymr	8	$38.79 \pm 0.25$ (?)
<b>Tarqeq</b>	<b>6</b>	<b><math>76.13 \pm 0.01</math></b>

*Notes:* Data are compiled from Tables 2 and 3 in [1], see also [7]. **Bold:** These moons orbit Saturn **progradely**. Other lines: Moons on retrograde orbits. The sizes (except Phoebe) are calculated from absolute magnitude  $H$  [8] with an assumed albedo  $A = 0.06$ ; they may be uncertain by ~30% to +50% due to uncertain values of  $A$  (approx.  $\pm 0.03$ ) and (to a lesser degree) of  $H$  (a few tenths of magnitude). Question marks indicate that the period is uncertain; in brackets that it is likely but not completely secure.

Some objects (Siarnaq, Ymir, Kiviuq) show lightcurve amplitudes  $>2$  mag at phase  $>60^\circ$ . The Tarqeq period is within 0.5% of the 1:5 resonance of Titan's orbit, raising the question of tidal influence.

### 3. Shape, binarity, pole, color

The number of lightcurve extrema gives hints on basic shapes of the moons. Potential first-order "end-member" shapes of Saturn's irregular moons are an "ellipsoid" (2-max/2-min lightcurves even at higher phase angles; e.g., seen at Kiviuq, Erriapus, Hati, or Bestla) and a "triangular prism" (3-max/3-min lightcurves also at lower phase as seen at Ymir, Siarnaq, Hyrokkin, and some others). Convex-shape models of Ymir and Siarnaq confirm this type of shape.

A possible interpretation of "triangular" convex shapes is that these objects might be contact-binary moons structured somehow similar to comet 67P/Churyumov-Gerasimenko. Furthermore, symmetric 2-max/2-min lightcurves with large amplitudes at low phase, slow rotational periods, plus other lightcurve structures qualify objects Kiviuq, Bestla, Erriapus, and possibly Bebhionn as binary-moon candidates.

The pole-axis of Ymir points close to the south-ecliptic pole, indicating a retrograde spin. For Siarnaq, an ecliptic lat/lon of  $\lambda, \beta = 98^\circ/-23^\circ \pm 15^\circ$  indicates that this moon experiences extreme seasons, somewhat reminiscent of the regular satellites of Uranus. For both moons, no hemispherical color variations could be detected on the surfaces.

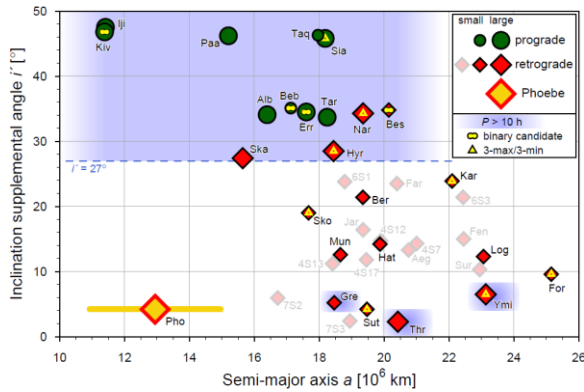


Figure:  $a$ - $i'$  plot for Saturn's irregular moons.

Notes: Adapted from [1]. The inclination supplemental angle  $i'$  ("orbit tilt") is defined as  $i' = 90^\circ - |90^\circ - i|$ . For Phoebe, periapsis and apoapsis are also shown (yellow bar). The bin "large" includes the 13 largest irregulars (separated at  $H = 14.4$  mag). Pale diamonds indicate moons not observed by Cassini (their rotational periods are unknown).

### 4. Patterns and correlations

Among Saturn's irregular moons, the orbital semi-major axes  $a$ , the orbital senses of motion (pro-/retrograde), the orbit tilts ( $i'$ ), the object sizes, and the rotational periods appear to be correlated to some degree. The prograde objects are on average closer to Saturn, on higher tilted orbits, larger in size, and slower rotators than the retrograde moons ( $\rightarrow$  Figure).

While the orbit stability is higher for retrograde objects than for progrades very far away from Saturn [9], a compelling physical cause for size and spin relations to orbital elements is not yet known. We may speculate that the progenitor objects had different material densities, with Phoebe being a potential source of one or several retrograde moon families.

### 5. Summary

The first ever photometric survey of irregular moons with an interplanetary spacecraft was performed with Cassini-Huygens. Disk-integrated observations of 25 irregular satellites of Saturn revealed that the individual objects are very different from each other. The data yielded rotational periods between  $\sim 1/4$  d and  $\sim 3$  d, and lightcurve amplitudes from 0.1 to 2.5 mag. They support the hypothesis that the irregulars are of low density and potentially cometary in nature. Binary or contact-binary moons are not proven, but may well be possible. Orbit ( $a$ ,  $i'$ ) and physical parameters (sizes, periods) appear to be correlated non-randomly, the cause is unknown.

### References

- [1] Denk T., Mottola S., Tosi F., Bottke W.F., Hamilton D.P. (2018): The irregular satellites of Saturn. In: *Enceladus and the Icy Moons of Saturn*. (Schenk, P.M. et al., eds.). 26 pp., Univ. of Arizona Press, Tucson, AZ.
- [2] Sheppard, S.S. (2006), *Asteroids, Comets, Meteors (ACM)*, Proceedings IAU Symposium No. 229, 319-334.
- [3] Jewitt, D., Haghighipour, N. (2007), *Annu. Rev. Astro. Astrophys.* 2007.45:261-295.
- [4] Nicholson, P.D., et al. (2008): Irregular Satellites of the Giant Planets. In: *The Solar System Beyond Neptune*, p. 411-424, Univ. of Arizona Press, Tucson, AZ.
- [5] Thomas, P.C., et al. (2018): The Inner Small Satellites of Saturn and Hyperion. In: *Enceladus and the Icy Moons of Saturn*, Univ. of Arizona Press, Tucson, AZ.
- [6] Bauer, J.M., et al. (2004), *Astrophys. J.* 610, L57-L60.
- [7] <https://tilmanndenk.de/outersaturnianmoons>
- [8] MPC ephemeris service: <http://www.minorplanetcenter.net/iau/NatSats/NaturalSatellites.html>
- [9] Nesvorný, D., et al. (2003), *Astron. J.*, 126, 398-429.

## **Saturn's deep atmosphere revealed by the Cassini Grand Finale gravity measurements**

**Eli Galanti** (1), Yohai Kaspi (1), Yamila Miguel (2), Tristan Guillot (3), Daniele Durante (4), Paolo Racioppa (4), and Luciano Iess (4)

(1) Weizmann Institute of Science, Rehovot, Israel, (2) Leiden University, The Netherlands, (3) Observatoire de la Cote d'Azur, Nice, France, (4) Sapienza Università di Roma, Rome, Italy

### **Abstract**

The Cassini Grand Finale gravity measurements, performed during May-July 2017, can shed light upon a longstanding question - what is the nature of the flow beneath Saturn's clouds? Answering this question has important implications not only for the atmospheric dynamics, but also for the interpretation of the interior density structure, composition, magnetic field and core mass. Strong zonal winds exist at the observed cloud-level, forming a wide superrotating region with winds of nearly 500 m/s at the equatorial region, and smaller scale jets extending to high latitudes, but whether these are superficial atmospheric structures or whether they extend deeply into the interior is unknown.

While the low-degree even gravity harmonics, as measured by Cassini, are dominated by the shape and density structure of the planet, the higher harmonics are found to be strongly influenced by differential flow and can be used to decipher its structure. In addition, the odd harmonics can be used for this purpose as they reflect solely the flow. Using Saturn's cloud-level winds and a thermal wind balance we relate the flow to the gravity harmonics. Then an adjoint based inverse model is used to determine the flow structure that gives the best fit between the model calculated gravity harmonics and those measured by Cassini. We present a first-order estimate of the flow structure based on the Cassini measurements, and discuss its implications to the planet's interior structure.



# On the carbon isotope ratio in Titan's atmosphere and interior

Vladimir A. Krasnopolsky

Moscow Institute of Physics and Technology (PhysTech), Moscow, Russia (vlad.krasn@verizon.net)

Please make sure that your pdf conversion results in a document with a page size of 237 x 180 mm!

## Abstract

To study the evolution of carbon on Titan,  $^{12}\text{C}/^{13}\text{C} = 89.7 \pm 1.0$  in methane should be compared to those in the precipitating haze and sputtering/ion escape. Calculations using the observed  $^{12}\text{C}/^{13}\text{C}$  in the photochemical products, their column rates of condensation and polymerization from the photochemical model, and data on sputtering/ion escape result in  $^{12}\text{C}/^{13}\text{C} = 88.5 \pm 3.0$  for the total loss of carbon. This loss of methane of  $7 \text{ kg cm}^{-2} \text{ Byr}^{-1}$  is probably replenished by outgassing/cryovolcanism of methane clathrate hydrate  $\text{CH}_4 \cdot 5.75\text{H}_2\text{O}$  with the above isotope ratio. Here we do not discuss some problems associated with this explanation.

## 1. Introduction

Carbon has two natural isotopes with  $^{12}\text{C}/^{13}\text{C} = 89.4$  on the Earth. Methane is the parent carbon species on Titan with mixing ratio decreasing from 5.7% near the surface to 1.5% above the tropopause at 75 km. Averaging a few measurements, the weighted-mean  $^{12}\text{C}/^{13}\text{C} = 89.7 \pm 1.0$  in methane on Titan (Nixon et al. [1]). The methane lifetime is rather short on Titan,  $\approx 30$  Myr. Nixon et al. [1] compared  $^{12}\text{C}/^{13}\text{C}$  in methane with that in the outer Solar System and evaluated the isotope fractionation in the loss of methane on Titan. Using data of three photochemical models, they concluded that methane was delivered into Titan's atmosphere 60-1600 Myr ago and its amount exceeded the present value by a factor 4-70. Mandt et al. [2] established an upper limit of 0.5 Byr to the outgassing timescale. Here we will use photochemical products to calculate the carbon isotope fractionation on Titan.

## 2. Initial data and models

$^{12}\text{C}/^{13}\text{C}$  in methane on Titan were measured using mass spectrometers at the Huygens probe [3] and the

Cassini flybys [2] as well as the CIRS spectra of the  $\text{CH}_4$  bands:

Table 1.  $^{12}\text{C}/^{13}\text{C}$  in methane on Titan

$^{12}\text{C}/^{13}\text{C}$	Instrument	Reference
$91.1 \pm 1.4$	Huygens/GCMS	Niemann et al. [3]
$88.5 \pm 1.4$	Cassini/INMS	Mandt et al. [2]
$86.5 \pm 8.2$	Cassini/CIRS	Nixon et al. [1]
$89.7 \pm 1.0$	Weighted-mean	

From Nixon et al. [1].

$^{12}\text{C}/^{13}\text{C}$  in the outer Solar System are equal to

Table 2.  $^{12}\text{C}/^{13}\text{C}$  in the outer Solar System

$^{12}\text{C}/^{13}\text{C}$	Species	Object	Reference
$92.6 \pm 4.3$	$\text{CH}_4$	Jupiter	Niemann et al. [4]
$91.8 \pm 8.1$	$\text{CH}_4$	Saturn	Fletcher et al. [5]
$90 \pm 4$	CN	comets	Hutsemekers et al. [6]
$91.3 \pm 2.7$	all	weighted-mean	
$92.4 \pm 5.4$	$\text{CH}_4$	weighted-mean	

Budget of methane in Titan's atmosphere is given in Table 3 based on our photochemical model [7]:

Table 3. Budget of methane on Titan [7]

Loss by photolysis	2.69+9	$k_{12}/k_{13} = 0$
Loss by $\text{C}_2\text{H} + \text{CH}_4$	1.62+9	1.019
Other loss	5.29+9	?
Total loss	9.60+9	
Production	1.13+9	?
Flow from surface	8.47+9	
	$7.09 \text{ kg cm}^{-2} \text{ Byr}^{-1}$	
Residence time	32.4 Myr	
$2.69 + 9 = 2.69 \times 10^9 \text{ cm}^{-2} \text{ s}^{-1}$ .		

Fractionation of carbon  $k_{12}/k_{13}$  was calculated by Nair et al. [8] for photolysis of methane and by Nixon et al. [1] for the reaction  $\text{C}_2\text{H} + \text{CH}_4 \rightarrow \text{C}_2\text{H}_2 + \text{CH}_3$ . Nixon et al. [1] adopted no fractionation in all other processes. Their calculations are based on comparison of  $^{12}\text{C}/^{13}\text{C}$  on Titan with that in the outer Solar System using the above reaction as the only

fractionation process. Mandt et al. [2] analyzed 30 Cassini/INMS flybys and obtained the isotope fractionation factor of methane escape at  $0.736 \pm 0.045$ . Using the Cassini/INMS observations, De la Haye et al. [9] evaluated the total loss of carbon from Titan by sputtering and ion escape at  $(2.8 \pm 2.1) \times 10^7 \text{ cm}^{-2} \text{ s}^{-1}$ .

### 3. Our model

The basic idea of our approach is to use  $^{12}\text{C}/^{13}\text{C}$  measured in photochemical products of methane (Table 4) as a tool to understand the carbon isotope fractionation.

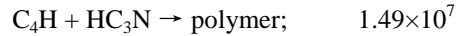
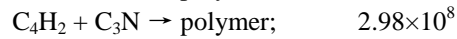
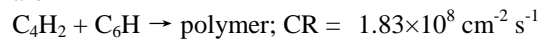
**Table 4.**  $^{12}\text{C}/^{13}\text{C}$  in photochemical products on Titan

Species	$^{12}\text{C}/^{13}\text{C}$	Instrument	C + P <sup>a</sup>
CO	$89.9 \pm 3.4$	ALMA [10]	-
C <sub>2</sub> H <sub>2</sub>	$84.8 \pm 3.2$	CIRS [11]	$3.12+8^b$
C <sub>2</sub> H <sub>6</sub>	$89.8 \pm 7.3$	CIRS [11]	$2.05+9$
C <sub>4</sub> H <sub>2</sub>	$90 \pm 8$	CIRS [12]	$1.98+9$
HCN	$89.8 \pm 2.8$	ALMA [13]	$1.47+8$
HC <sub>3</sub> N	$79 \pm 17$	CIRS [14]	$1.13+9$
CO <sub>2</sub>	$84 \pm 17$	CIRS [15]	$1.78+6$
All	$88.3 \pm 1.8$	weighted-mean (uncertainties)	
All	$88.3 \pm 3.0$	wiegheted-mean	

<sup>a</sup> Condensation plus polymerization from table 1 and 4 in [7], in numbers of carbon atoms.

<sup>b</sup>  $3.12+8 = 3.12 \times 10^8 \text{ cm}^{-2} \text{ s}^{-1}$ .

Usually the measured isotope ratios are weighted by their uncertainties, and the weighted-mean  $^{12}\text{C}/^{13}\text{C}$  is  $88.3 \pm 1.8$ . However, another important factor is the contribution of each species to production of the haze by condensation and polymerization. These data are taken from the photochemical model [7]. The most significant reactions of polymerization in the model are



Here CR is the column rate, and we adopt that  $^{12}\text{C}/^{13}\text{C}$  in C<sub>4</sub>H and C<sub>3</sub>N are equal to those in C<sub>4</sub>H<sub>2</sub> and HC<sub>3</sub>N, respectively. The calculated weighted-mean carbon isotope ratio is  $88.3 \pm 3.0$  in the haze on Titan. Comparing with the isotope ratio of methane, the haze is slightly enriched in heavy carbon. This conclusion is opposite to that in [1] and agrees with the recent laboratory simulations of Titan's haze (Sebree et al. [16]).

A minor correction for sputtering and ion escape results is  $^{12}\text{C}/^{13}\text{C} = 88.5 \pm 3.0$  for a source of methane

that compensate for its loss. That may be outgassing and/or cryovolcanism of, say, methane clathrate hydrate CH<sub>4</sub>\*5.75H<sub>2</sub>O. However, there are some difficulties associated with this explanation (see for example [1]).

Another scenario with injection of, e.g., ten times the present methane abundance  $\approx 300$  Myr ago and its gradual decrease by the photochemistry, results in  $^{12}\text{C}/^{13}\text{C} = 87.1 \pm 7$  for the injected methane. Compared with the permanent outgassing, this scenario is less favorable in both the assumption and the result (the greater difference between the isotope ratio and that in the outer Solar System). Another scenario with a constant outgassing that started some time ago is an intermediate case. Evidently its result is intermediate as well.

**Acknowledgement.** This work is supported by a grant of Russian Science Foundation to Moscow Institute of Physics and Technology (PhysTech) and V.A. Krasnopolsky.

### References

- [1] Nixon C.A. et al. *Astrophys. J.* 759, 159, 2012.
- [2] Mandt K. et al. *Astrophys. J.* 759, 160, 2012.
- [3] Niemann H.B. et al. *JGR* 115E, E12006, 2010.
- [4] Niemann H.B. et al. *JGR* 103, 22831, 1998.
- [5] Fletcher L.N. et al. *Icarus* 199, 351, 2009.
- [6] Hutsemekers H. et al. *Astron. Astrophys.* 440, L21, 2005.
- [7] Krasnopolsky V.A. *Icarus* 236, 83, 2014.
- [8] Nair H. et al. *Icarus* 175, 32, 2005.
- [9] De la Haye V. et al. *JGR* 112, A07309, 2007.
- [10] Serigano J. et al. *Astrophys. J. Lett.* 821, L8, 2016.
- [11] Nixon C.A. et al. *Icarus* 195, 778, 2008.
- [12] Jolly A. et al. *Astrophys. J.* 714, 852, 2010.
- [13] Molter E.M. et al. *Astron. J.* 152, 42, 2016.
- [14] Jennings D.E. et al. *Astrophys. J. Lett.* 681, L109, 2008.
- [15] Nixon C.A. et al. *Astrophys. J. Lett.* 681, L101, 2008.
- [16] Sebree J.A. et al. *Icarus* 270, 421, 2016.

# Equatorial magnetic field oscillations observed over the Cassini mission

**D. J. Andrews** (1), S. W. H. Cowley (2), L. Z. Hadid (1), G. Hunt (3), M. Morooka (1), G. Provan (2) and J.-E. Wahlund (1)  
 (1) Swedish Institute for Space Physics, Uppsala, Sweden (david.andrews@irfu.se), (2) Department of Physics & Astronomy, University of Leicester, UK  
 (3) Blackett Laboratory, Imperial College, London, UK.

## Abstract

Two systems of “Planetary Period Oscillations” (PPO) are found in Saturn’s magnetosphere, associated with the Northern (N) and Southern (S) hemispheres. In all data sets (magnetic, radio, plasma), they display an  $m=1$  azimuthal wavenumber, rotating in the same sense as the planet, albeit at subtly different periods depending on the source hemisphere. Secular changes in their period and relative amplitude are seen. Andrews et al., 2010 produced a first “map” of the equatorial PPO magnetic field structure, but their results only reflected the then dominant Southern system. Here, we revisit this study of the structure of these oscillating fields in the equatorial magnetosphere, to take account of improved understanding of PPOs. We show updated, completed “maps” of both the Northern, Southern and “Mean” magnetic field oscillation structures. From these we compute field-aligned current densities.

## 1. Observations

Using a suitable guide phase, we determine the amplitude and phase of the PPO fields from near-equatorial Cassini magnetometer data by first removing the internal magnetic field of the planet, and then applying a band-pass filter. The data are then grouped into spatial bins on the equatorial plane, and amplitudes and phases determined in each bin.

$$B_i(r, \varphi, t) = B_{i0}(r, \varphi) \cos [\Phi(t) - \varphi - \psi_i(r, \varphi)]$$

Field Amplitude (fit)
Azimuth (LT) of Cassini  
Guide Phase
Spatial Phase (fit)

Framework for description of PPO fields.

In Figure 1 we show results determined using the southern hemisphere guide phase at a particular instant in the oscillation cycle. The overall picture is consistent with that obtained by Andrews et al., [2010], with

distributed regions of upward and downward centered at  $12-15 R_S$ , evidenced by the sense of the curl in the field vectors.

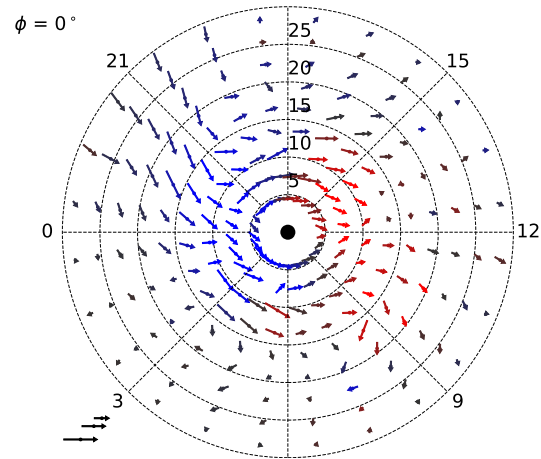


Figure 1: Plots of Saturn’s equatorial PPO field associated with the southern hemisphere system.

In Figure 2 we use instead a guide phase appropriate to the northern hemisphere system, and independently obtain the structure of the equatorial PPO fields associated with the second system of rotating currents. The general structure is clearly very similar to that of the southern system, with the sense of the parallel component of the field (blue / red in the figure) reversed as expected. Regions of upward and downward field aligned current are found at broadly similar local times (at this phase of the cycle), but are somewhat less well resolved.

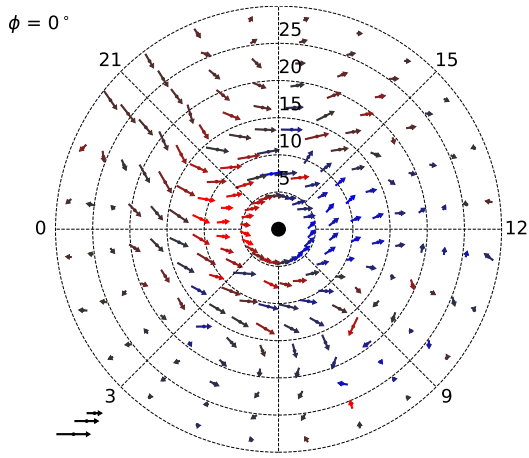


Figure 2: Plots of Saturn's equatorial PPO field associated with the northern hemisphere system.

## 2 Summary

1. Full picture of the equatorial magnetic field oscillations associated with the PPO current system obtained
2. Southern hemisphere system essentially as reported previously by Andrews et al., [2010]
3. Equivalent northern hemisphere fields are as expected on the basis of the PPO current system deduced from higher-latitude Observations

## Acknowledgements

Work at IRF was supported by grants from the Swedish National Space Agency (DNR 162/14). All data used in this paper are available in the ESA planetary science archive, <https://archives.esac.esa.int/psa>.

## References

[Andrews et al., (2010)] Andrews, D. J., S. W. H. Cowley, M. K. Dougherty, and G. Provan (2010), Magnetic field oscillations near the planetary period in Saturn's equatorial magnetosphere: Variation of amplitude and phase with radial distance and local time, *J. Geophys. Res.*, *115*, A04212, doi: 10.1029/2009JA014729.

# Cassini: One Year Later

**Linda J. Spilker** and Scott G. Edgington, Jet Propulsion Laboratory, California Institute of Technology, Pasadena, United States ([linda.j.spilker@jpl.nasa.gov](mailto:linda.j.spilker@jpl.nasa.gov), [scott.g.edgington@jpl.nasa.gov](mailto:scott.g.edgington@jpl.nasa.gov)).

## Abstract

Cassini, the most distant planetary orbiter ever launched, arrived at Saturn in 2004. For the next 13 years, through its prime and two extended missions, and over almost half a Saturnian year, this spacecraft made astonishing discoveries, reshaping and fundamentally changing our understanding of this unique planetary system. Cassini sent back its final bits of unique science data on 15 September 2017, as it plunged into Saturn's atmosphere, vaporizing and satisfying planetary protection requirements.

During its last year of exploration, Cassini completed its investigations of the Saturn system, probed as-yet unsolved mysteries, observed seasonal and temporal changes, and addressed new questions that arose during the mission, some of which could only be answered during the final, unique orbits plunging between the rings and planet. Science highlights and new mysteries gleaned from the Ring Grazing and Grand Finale orbits will be discussed.

## 1. Key Mission Highlights

*Titan, Earth-like world:* Less than a year after arrival, Cassini released Huygens, the European Space Agency's parachuted probe built to study the atmosphere and surface of Titan. The Huygens probe became the first human-made object to land on an outer solar system moon. The probe's descent provided the first in situ measurements of atmospheric temperature, pressure and composition, and provided the first detailed images of the surface. Huygens revealed Titan's surface to be remarkably Earth-like and other Cassini instruments also found that Titan has many geologic processes reminiscent of those on Earth. These processes generate methane clouds and rain, build river channels, form lakes and seas containing liquid methane and ethane, form complex atmospheric hydrocarbons, and generate dunes of hydrocarbon particles. Cassini also detected a subsurface ocean on Titan.

*Enceladus, an ocean world:* Cassini's revolutionary findings at tiny Enceladus included icy jets of material shooting from Enceladus' four south

polar fractures, or "tiger stripes", and a subsurface, global, salty ocean containing organics, ammonia, hydrogen, and silicates, with active hydrothermal vents on its seafloor. Cassini revealed an ocean world that is potentially habitable. These discoveries have fundamentally altered many of our concepts of where life may be found in our solar system. Enceladus is also the source of the E Ring and water from its jets dominates the Saturnian magnetosphere.

*Dynamic Rings:* Cassini's 13 years in orbit made it possible to observe temporal changes in Saturn's dynamic ring system. The orbiter discovered migrating propeller-like objects and unexpected ring particle clumping, imaged the possible birth of a new moon at the edge of the A ring, and observed one of the most active, chaotic rings in our solar system, Saturn's F ring. Ring processes provide a laboratory for how planets might form.

*Saturn's storms:* Cassini discovered hurricane-like storms centered at each pole. Around the north polar hurricane is a long-lived hexagonal-shaped jet stream that is two Earth diameters across. The source of this six-sided jet stream still remains a mystery. Cassini also provided multiwavelength coverage of a great northern storm that began in 2010, the first of its kind on Saturn since 1990. Within months, this storm completely encircled the planet with a swirling band of clouds and vortices, fading away nine months later, shortly after the main vortex in its head collided with one in its tail.

*Saturn's Internal Rotation Rate:* Saturn's Kilometric Radiation (SKR) was first observed by Voyager in the 1980's and used to make an initial calculation of Saturn's internal rotation period. However, when Cassini arrived at Saturn and measured the SKR period, data from the radio and plasma wave instrument showed that the variation in radio waves was different in the northern and southern hemispheres. Clearly the observations of SKR were not coming from the interior but are an atmospheric signal. It remained for magnetic field measurements taken during the Grand Finale orbits to attempt to solve this puzzle.

Many other fascinating discoveries were made by the Cassini orbiter and Huygens probe that are the subjects of numerous papers and books.

## 2. Cassini's Final Orbits

Cassini's ocean world discoveries required a mission end that would not allow the spacecraft to impact and potentially contaminate Saturn's ocean worlds once Cassini was out of fuel and could no longer navigate the Saturn system.

*Ring Grazing Orbits.* In late 2016, a close flyby of Titan changed Cassini's trajectory to a series of 20 Ring Grazing orbits with peripases located within 10,000 km of Saturn's F ring (Figure 1, gray orbits). These orbits provided some of the mission's highest-resolution views of Saturn's F ring, and A and B rings, and prime viewing conditions for fine scale ring structures such as propellers and wispy clumps in the rings. They also included the closest flybys of tiny ring moons, including Pan, Daphnis and Atlas, and remarkable views of the Daphnis-created wave on the edge of the Keeler gap. Plasma and dust composition measurements were also conducted in this region.

*Grand Finale Orbits.* In late April 2017, a final close flyby of Titan propelled Cassini across Saturn's main rings and into its Grand Finale orbits. The spacecraft repeatedly dove between Saturn's innermost rings and upper atmosphere for 22 orbits (Figure 1, blue orbits) attempting to answer fundamental questions unattainable earlier in the mission. The Grand Finale represented a brand-new mission, exploring a region of the Saturn system that was unexplored by any previous outer planet spacecraft.

Saturn's gravitational field was measured to unprecedented accuracy, providing information from which constraints on the interior structure of the planet, winds in the deep atmosphere, and mass distribution in the rings could be derived. Probing the magnetic field provided insight into the physics of the magnetic dynamo, the structure of the internal magnetic field, the location of the metallic hydrogen transition region and Saturn's internal rotation period.

The Grand Finale orbits provided the highest resolution observations ever of both Saturn's C and D rings and Saturn's atmospheric weather layer. Direct in-situ sampling of the ring particle composition and the innermost radiation belts was also achieved. The ion and neutral mass spectrometer sampled the exosphere and upper atmosphere for molecules entering and escaping from the atmosphere and water-based molecules originating from the rings.

The cosmic dust analyzer directly sampled the composition of ring particles from different regions of the main rings for the first time.

*Cassini's Final Half-orbit.* The last orbit turned the spacecraft into the first Saturn atmosphere probe with all of fields and particle instruments gathering data as long as the spacecraft remained stable. Approximately one additional scale height of atmosphere was probed prior to loss of the radio signal from the spacecraft.

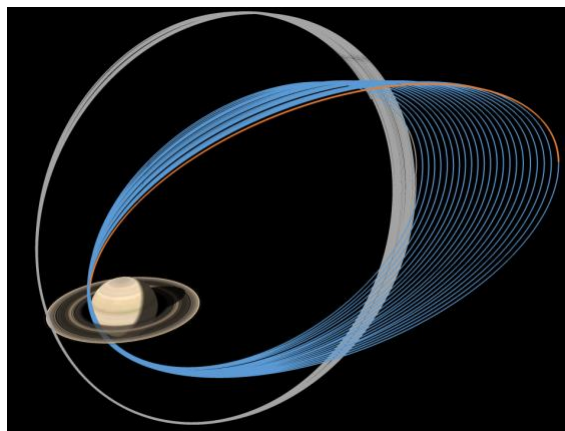


Figure 1: Cassini's 20 Ring Grazing (gray) and Grand Finale (blue) orbits. The last orbit (orange) plunged Cassini into Saturn's atmosphere.

## 3. Summary

Cassini-Huygens exploration of Saturn has yielded 13 years of unprecedented discoveries and answers to many scientific mysteries, in addition to revealing potentially habitable ocean worlds. The final phase of the mission ended with the first in-situ exploration of the region between the rings and planet.

## Acknowledgements

We would like to gratefully acknowledge all of the Cassini team members who designed, developed and operated the Cassini-Huygens mission, which is a joint collaboration of NASA, the European Space Agency (ESA), and the Italian Space Agency (ASI) and is managed by JPL/Caltech under a contract with NASA. The work described here was carried out in part at the Jet Propulsion Laboratory, California Institute of Technology, under a contract with the National Aeronautics and Space Administration. Copyright 2018 California Institute of Technology. Government sponsorship is acknowledged.



# Saturn's ionosphere: Electron density altitude profiles and ring shadowing effects from the Cassini Grand Finale.

L. Z. Hadid (1), M. W. Morooka (1), J-E. Wahlund (1), A. M. Persoon (2), D. J. Andrews (1), O. Shebanits (3), W. M. Farrell (4), W. S. Kurth (2), N. J. T. Edberg (1), E. Vigren (1), L. Moore (5), M. M. Heddman (6), T. E. Cravens (7), A. F. Nagy (8), A. I. Eriksson (1)

(1) Swedish Institute of Space Physics, Uppsala, Sweden, (2) Department of Physics and Astronomy, University of Iowa, USA, (3) Space and Atmospheric Physics, Imperial College, UK, (4) NASA/Goddard Space Flight Center, Maryland, USA, (5) Center for Space Physics, Boston University, USA, (6) Department of Physics, University of Idaho, USA, (7) Department of Physics and Astronomy, University of Kansas, USA, (8) Climate and Space Sciences and Engineering, University of Michigan, USA. ([lina.hadid@irfu.se](mailto:lina.hadid@irfu.se))

## Abstract

Using the latest *in-situ* measurements of the Langmuir probe (LP) part of the Radio & Plasma Wave Science (RPWS) instrument package onboard the Cassini spacecraft, we analyse the electron density altitude profiles of all the proximal orbits from the Cassini Grand Finale.

Firstly, we study the electron density ( $n_e$ ) altitude ( $h$ ) profile by comparing the northern and the southern hemispheres. We construct an average ionospheric profile in the northern hemisphere and show a layered structure. Similar layers were observed during the Final Plunge of Cassini, where the main ionospheric peak is crossed at  $\sim 1550$  km altitude [1]. Secondly, from the ring shadow signatures on the total ion current, we reproduce the A and B ring boundaries and confirm some of their optical properties. Furthermore, observed variable response of the ionosphere to the B ring shadow implies different proton production rate and plasma transport from the C-D rings [2].

## 1. Electron density altitude profile model

We show in Figure 1-a the consecutive  $h$ ,  $n_e$  profiles of all the proximal orbits measured by the LP and for some cases estimated from the plasma wave frequency characteristics of the RPWS investigation. The black line represents the averaged topside ionospheric profile up to 5500 km. As one can see, it exhibits a layered structure with distinct regions denoted by **P** ( $h > 4000$  km), **D** ( $2200 \text{ km} \lesssim h \lesssim 4000 \text{ km}$ ) and **C** ( $h < 2200 \text{ km}$ ). Region **P**, which we interpret as the inner part of the plasma-sphere, is characterized by near-constant  $n_e$  values with respect to altitude before it starts to increase around 4500 km. Region **D** represents a diffusive equilibrium region, it is highly variable and structured. Region **C**, which is a chemical equilibrium layer, is more stable and regular and dominated by heavy ions [3, 4].

In Figure 1-b, we present the “Final Plunge” orbit. One can clearly relate the three

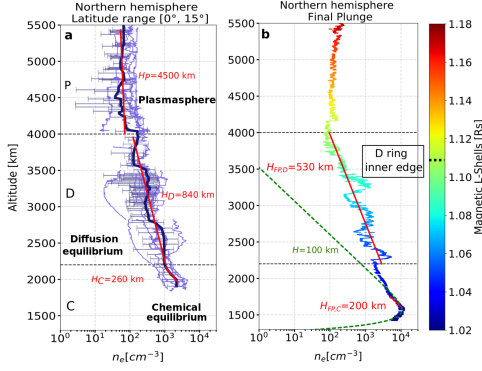


Figure 1: (a) The averaged  $h, n_e$  profile (dark blue curve) over all the proximal orbits (purple curves) in the northern hemisphere. (b) The  $h, n_e$  profile of the Final Plunge orbit. The color code shows the corresponding magnetic L-Shell values.

different ionospheric regions highlighted in the averaged profile. The color code corresponds to the magnetic L-Shell values and shows that region **D** maps well inside the inner edge of the D ring. This implies that the observed irregularities density profiles in layer **D** not connected to features in the rings. The red lines represent the estimation of the plasma scale height by fitting with an exponential curve for each of the regions **P**, **D** and **C**. Last but not least, during the Final Plunge orbit the LP have revealed a density peak of  $\sim 1.5 \times 10^4 \text{ cm}^{-3}$  around 1550 km, which we interpret as the “main peak” of the Kronian ionosphere.

## 2. A and B ring shadowing effects

As Saturn’s northern hemisphere experienced summer during the Grand Finale, the planet’s northern dayside hemisphere and its rings were fully illuminated by the sun. However

the southern hemisphere was partly obscured because of the shadows cast by the A and B rings, which are opaque to the Extreme Ultraviolet (EUV) solar radiation. As a consequence, this caused noticeable decrease in the amount of ionization in the southern portion of the ionosphere which was clearly observed by a decrease in the total DC ion current ( $I_{DC,tot}$ ) collected by the LP (blue curve in Figure 2).

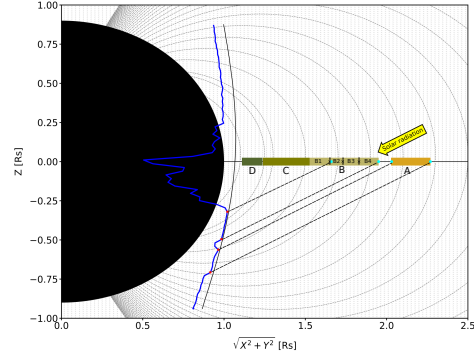


Figure 2: Example of one proximal orbit (Rev 276) passing between Saturn (in black) and the rings (green rectangles). The blue curve represents the total DC current for negative bias voltage projected on the orbit.

As is shown in Figure 2, considering a solar elevation angle of  $26.3^\circ$ , we project the outbound slant passes (larger for local times away from noon) onto the ring plane, and compare the observed projected boundaries of the shadowed regions (blue dots) with the ring boundaries.

In Figure 3 we summarize the distances from Saturn of the observed starting and ending points of the shadows compared with the A and B ring boundaries (black dashed lines). The color code represents the total DC current. Based on the current values, we consider the LP in complete shadow when the



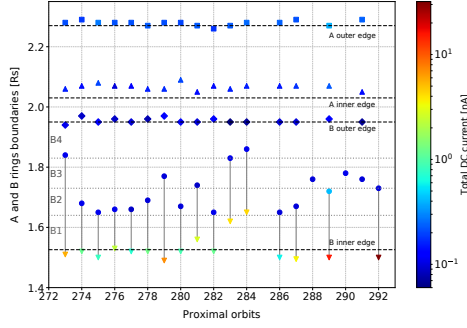


Figure 3: Summary of the observed inner and outer edges of the shadows casted by the A (triangle and square respectively) and the B rings (circle and diamonds respectively). The dashed black lines represents the inner and outer boundaries of the A and B rings.

collected current is below the photoelectron level ( $< 0.7$  nA) or around the noise level (0.1 nA). As one can see, the observed edges of the shadow cast by the A ring (squares and upward triangles) match very well with its boundaries. Regarding the B ring, the observed outer edges of the shadow (Diamonds) match the outer edge of the ring consistently from one flyby to another. However this is not the case for the inner edges of the shadow (circles), they are neither uniform nor matching the B ring inner boundary. For each orbit, we represent by a downward triangle the distance at which  $I_{DC,tot}$  starts to decrease and by a circle the distance at which the LP is shadowed by the B ring ( $I_{DC,tot} \sim 0.1$  nA). For most the flybys,  $I_{DC,tot}$  starts to decrease around the inner edge of the B ring.

The observed variations in the starting point of the B ring shadow around 4000 km, for distances outside  $1.65 R_s$ , could be related to the changes of the proton production rate resulting in different responses of the molecular hydrogen to the shadowing effect. Further-

more, plasma transport processes from/to the rings could also inhibit the shadowing signature from the B ring.

### 3. Summary

This study has provided detailed analysis of the Kronien topside ionosphere by evidencing a layered structure with at least a diffusive and chemical equilibrium regions. Moreover, based on the observed A and B ring shadows we could study the reponses of the ionospheric plasma in the absence of the sunlight as an ionization source.

### References

- [1] Hadid, L. Z., Morooka, M. W., Wahlund, J.-E., Persoon, A. M., Andrews, D. J., Shebanits, O., Kurth, W. S., Vigren, E., Edberg, N. J. T., Nagy, A. F., and Eriksson, A. I., (2018), *Geophysical Research Letters*, submitted.
- [2] Hadid, L. Z., Morooka, M. W., Wahlund, J.-E., Moore, L., Cravens, T. E., Hedman, M. M., Edberg, N. J. T., Vigren, E., Kurth, W. S., Farrell, W. M., and Eriksson, A. I., (2018). *Geophysical Research Letters*, submitted.
- [3] Morooka, M. W., Wahlund, J.-E., Hadid, L. Z., Edberg, N. J. T., Vigren E., Andrews, D. J., Persoon, A. M., Kurth, W. S., Gurnett, D. A., Farrell, W. M. Waite, J. H., Perryman, R. S., Perry, M., Mitchell, D. G. and Hsu, S. (2018). *Geophysical Research Letters*, submitted.
- [4] Waite, J.H., Jr., R. Perryman, M. Perry, K. Miller, J. Bell, T.E. Cravens, C.R. Glein, J. Grimes, M. Hedman, T. Brockwell, B. Teolis, L. Moore, D. Mitchell, A. Persoon, W.S. Kurth, J.-E. Wahlund, M. Morooka, L. Z. Hadid, S. Chocron, J. Walker, A. Nagy, R. Yelle, S. Ledvina, R. Johnson, W. Tseng, O.J. Tucker and W.-H. Ip (2018), *Science*, submitted.

## Saturn's Equatorial Ionosphere as Observed by Cassini: Composition and Flow

**T. E. Cravens** (1), A. Renzaglia (1), L. Moore (2), J. H. Waite Jr. (3), R. Perryman (3), M. Perry (4), J.-E. Wahlund (5), L. Hadid (5), and A. Persoon (6)

(1) Department of Physics and Astronomy, University of Kansas, Lawrence, KS 66045, USA, (2) Center for Space Physics, Boston University, Boston, MA 02215, USA, (3) Southwest Research Institute, Space Science and Engineering Division, 6220 Culebra Road, San Antonio, TX 78238, USA, (4) Applied Physics Laboratory, Johns Hopkins University, Laurel, MD 20723, USA, (5) Swedish Institute of Space Physics, Box 537, SE-751 21 Uppsala, Sweden, (6) Department of Physics and Astronomy, University of Iowa, Iowa City, IA 52242. (cravens@ku.edu)

### Abstract

The Cassini Orbiter measured the upper atmosphere and ionosphere of Saturn in 2017. Molecular hydrogen and helium were the major neutrals seen by the Ion and Neutral Mass Spectrometer (INMS) but important minor species were also seen including water, methane, ammonia, and organics. INMS in its ion mode measured light ion species ( $H^+$ ,  $H_2^+$ ,  $H_3^+$ ,  $He^+$ ) and the Radio and Plasma Wave Science (RPWS) instrument measured electron densities in the ionosphere. The spacecraft (s/c) velocity with respect to Saturn during the proximal orbits was 31 km/s, which corresponds to 25 times higher kinetic energy per nucleon for incident molecules than during the Titan encounters. Heavier neutral species, or even grains, break up in the closed source antechamber at these speeds and INMS ion measurements were limited to species with mass numbers less than 8 Daltons (i.e., only lighter ions). The chemistry and dynamics of Saturn's ionosphere will be discussed using Cassini data and simple theory.

### 1. Photochemical Analysis

Photochemistry plays a key role in the main ionospheric layer of Saturn. Analysis shows that photoionization of molecular hydrogen is the main source of plasma. The  $H_2^+$  ions produced react with  $H_2$  to produce  $H_3^+$  and  $H_3^+$  ions can dissociatively recombine. But theoretical  $H^+$  and  $H_3^+$  densities greatly exceed the measured densities unless another chemical loss process is operating. A quantitative explanation of the measured  $H^+$  and  $H_3^+$  densities requires that they chemically react with one or more heavy neutral molecular species that have mixing ratios of about of 100 parts per million (Cravens et al., 2018, and Moore et al., 2018). This is consistent with the neutral measurements made by INMS showing the presence in the upper atmosphere of

neutral species (e.g., methane) and/or grains thought to originate in the rings (Waite et al., 2018 and Perry et al., 2018).

A photochemical analysis of the INMS and RPWS data indicates that the major ion species near the ionospheric peak must be heavy and molecular with a short chemical lifetime (e.g.,  $CH_3^+$ ).

### 2. Dynamical Analysis of the Ionosphere

Photochemical lifetimes increase with increasing altitude in the ionosphere whereas ion transport times become shorter. Understanding the distribution of ionospheric plasma requires the inclusion of transport effects. INMS data shows that  $H^+$  is the major ion species in the topside Saturn ionosphere at high altitudes, and RPWS data shows interesting structure associated either with altitude and/or latitude. During one of the Cassini proximal orbits energy scans were performed using the INMS ion optics which allowed  $H^+$  flow speeds along the spacecraft track to be measured. This data will be presented and shows a flow along the magnetic field from the northern hemisphere to the southern hemisphere.

A simple numerical dynamical model of the ionosphere is used to interpret INMS and RPWS data. Single species fluid equations are numerically solved along magnetic field lines and the model includes chemical production and loss, and ion-neutral collisions. The effects of ring shadowing (Hadid et al. 2018) are included in the model and are necessary to explain the data.

# Can the Alkanofer of Titan show a chemical stratification?

D. Cordier (1) and M. Coutelier (1)

(1) Groupe de Spectrométrie Moléculaire et Atmosphérique - UMR CNRS 7331 Campus Moulin de la Housse - BP 1039  
Université de Reims Champagne-Ardenne 51687 REIMS – France

## Abstract

Titan, the enigmatic large moon of Saturn, is the unique satellite of the solar system surrounded by a dense atmosphere. In polar regions, lakes and seas of liquid hydrocarbons have been discovered by *Cassini/Huygens* mission. Thanks to the analysis of radar data, acquired during numerous flybys, it has been recently demonstrated that several liquid bodies have their surfaces at the same equipotential. These altimetric determinations suggest strongly the existence of a kind of subsurface connection between some lakes or maria. In the present work, we investigate the properties of a possible alkanofer, made of a cryogenic liquid mixture, trapped into a porous icy crust. We pay particular attention to the fate of ethane, the main product of atmosphere chemistry, in such a context.

## 1. Introduction

Titan, the main satellite of Saturn, is the only satellite of the solar system possessing a dense atmosphere. The latter, which composition is dominated by nitrogen and methane, harbors a complexe chemistry initiated by the photolysis of these species. Among a plethora of molecules, ethane dominates the products of the atmosphere chemistry. Since the *Voyager* flyby, the existence of liquid bodies at the surface of Titan has been suspected. Thanks to its radar, which had the capability of imaging the surface through the atmosphere opaque to visible light, the *Cassini* orbiter instruments have revealed a collection of dark features dotting the polar regions (Stofan et al., 2007; Turtle et al., 2009). These geomorphological characteristics are interpreted as lakes or seas (depending on their size) of liquid hydrocarbons. These structures were found at both poles and involve diameters up to more than hundreds of kilometers.

Recently, Titan's surface altimetry investigations have shown that several Maria share the same equipotential for their free surface (Corlies et al., 2017; Hayes et al., 2017). These new measurements suggest the ex-

istence of some local subsurface connectivity between liquid bodies. The concept of *alkanofer*, analog of terrestrial aquifer, has been already proposed in the literature (Mousis et al., 2014, 2016). Such *alkanofer* consists of a mixture of liquid hydrocarbons trapped in a porous icy crust.

On the Earth, beside already mentioned aquifers, "alkanofers" also exist and are called "hydrocarbon reservoirs", they contain petroleum and gases. For many decades, field measurements have revealed a wide range of compositional variation in these reservoirs. These variations are most of the time vertical (Metcalf et al., 1988), while horizontal cases are also observed. In general, lighter hydrocarbon are found at the top of the reservoir, while the heaviest molecules are buried at the bottom of the system. The analysis and modeling of such compositional grading is of primary importance for the oil and natural gases industry. In the context of Titan, one may wonder whether such a chemical stratification could appear within an alkanofer mainly composed by a liquid mixture of methane and ethane, under Titan's cryogenic conditions and low gravity.

## 2. The Diffusion of Species through Titan's Alkanofer

Since the convection is often inhibited in hydrocarbon reservoirs, the transport process at work is based on diffusion processes. In the general case, the total diffusion mass flux  $\vec{j}_1$  ( $\text{kg m}^{-2} \text{s}^{-1}$ ) of one of the two components making a binary mixture, may be written (Bird et al., 1960; Ghorayeb & Firoozabadi, 2000)

$$\vec{j}_1 = -\rho D_{12} \frac{M_1 M_2}{M^2} \left\{ \left. \frac{\partial \ln f_1}{\partial \ln x_1} \right|_{P,T} \vec{\nabla} x_1 + \frac{x_1}{RT} \left( \bar{V}_1 - \frac{M_1}{\rho} \right) \vec{\nabla} P + \frac{k_{T,1,2}}{T} \vec{\nabla} T \right\} \quad (1)$$

with  $\rho$  the density ( $\text{kg m}^{-3}$ ) of the mixture,  $D_{12}$

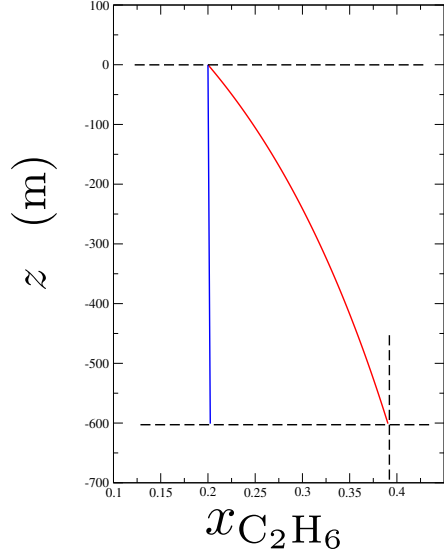


Figure 1: Red line: the ethane mole fraction as a function of depth ( $z$  in m) for a semi-ideal model. Blue line: the same thing for a non-ideal model based on the equation of state PC-SAFT.

the Fickian diffusion coefficient ( $\text{m}^2 \text{s}^{-1}$ ) of species (1) in a “bath” of species (2),  $M_1$  and  $M_2$  the respective molecular weights ( $\text{kg mol}^{-1}$ ) of involved species (here: (1)  $\text{C}_2\text{H}_6$  and (2)  $\text{CH}_4$ ), while  $\bar{M}$  is the average molecular weight of the system:  $\bar{M} = x_1 M_1 + (1 - x_1) M_2$ . The fugacity, which measures non-ideal effects for a real gas, is represented by  $f_1$ . Adopting an usual notation,  $x_1$  and  $\bar{V}_1$  are the mole fraction of species (1) and its molar volume ( $\text{m}^3 \text{mol}^{-1}$ ),  $P$  and  $T$  are respectively the local pressure (Pa) and temperature (K). In the last term, the thermal diffusion ratio  $k_{T1,2}$  (pure number) is a function of  $\alpha_{T1,2}$  (pure number) the thermal diffusion coefficient  $k_{T1,2} = \alpha_{T1,2} x_1 (1 - x_1)$ .

If in a first approach we neglect the effect of thermal diffusion (third term in the right hand side of Eq. 1), at the equilibrium (*i.e.* when  $\vec{j}_1 = \vec{0}$ ), the system to be solved becomes

$$\left. \frac{\partial \ln f_1}{\partial \ln x_1} \right|_{P,T} \frac{\partial x_1}{\partial z} = \frac{x_1}{RT} \left( \bar{V}_1 - \frac{M_1}{\rho} \right) \rho g_{\text{Titan}} \quad (2)$$

$$\frac{\partial P}{\partial z} = -\rho g_{\text{Titan}}$$

where  $\partial x_1 / \partial z$  is the vertical gradient of ethane, and  $g_{\text{Titan}}$  the Titan gravity. The results of this first approach are gathered in Fig. 1, while the semi-ideal model, *i.e.* neglecting almost all intermolecular interactions, shows a massive enrichment in ethane 600 meters below the surface; the non-ideal model, based on the equation of state PC-SAFT produces outputs in which the mixture remains well homogeneous. By adding a certain amount of dissolved nitrogen, we do not change this result at all. The explanation of the uniformity of ethane concentration could be the intermolecular interaction that “force” the molecules to remain mixed, letting the gravity having a purely negligible influence.

### 3. Summary

In this presentation, we will discuss the influence of factors that could alter the vertical gradient of ethane in the possible Titan’s alkanofor. We will particularly focus on the influence of temperature. Other species will be also reviewed.

### References

- Bird, R. B. and Stewart, W. E. and Lightfoot, E. N., 1960, *Transport Phenomena*, John Wiley and Sons, New York.
- Corlies, P. and Hayes, A. G. and Birch, S. P. D. and Lorenz, R. and Stiles, B. W. and Kirk, R. and Poggiali, V. and Zebker, H. and Iess, L. 2017, GRL, 44, 11.
- Ghorayeb, K. and Firoozabadi, A. 2000, AIChEJ, 46, 883.
- Hayes, A. G. and Birch, S. P. D. and Dietrich, W. E. and Howard, A. D. and Kirk, R. L. and Poggiali, V. and Mastrogiuseppe, M. and Michaelides, R. J. and Corlies, P. M. and Moore, J. M. and Malaska, M. J. and Mitchell, K. L. and Lorenz, R. D. and Wood, C. A. 2017, GRL, 44, 11.
- Metcalf, R. S. and Vogel, J. L. and Morris, R. W. 1988, SPE.
- Mousis, O. and Choukroun, M. and Lunine, J. I. and Sotin, C. 2014, Icarus, 239, 39.
- Mousis, O. and Lunine, J. I. and Hayes, A. G. and Hofgartner, J. D., Icarus, 270, 37.
- Stofan, E. R., Elachi, C., Lunine, J. I., et al. 2007, Nature, 445, 61
- Turtle, E. P., Perry, J. E., McEwen, A. S., et al. 2009, Geophys. Res. Lett., 36, 2204

# Saturn's stratospheric thermal structure, composition and dynamics revealed by Cassini/CIRS limb observations

**Sandrine Guerlet** (1), T. Fouchet (2), M. Sylvestre (3), A. A. Simon (4), G. Bjoraker (4) and F. M. Flasar (4).  
(1) Laboratoire de Météorologie Dynamique (LMD), Paris, France (2) LESIA, Observatoire de Paris, Meudon, France (3) University of Bristol, Bristol, UK, (4) NASA Goddard Space Flight Center, Greenbelt, MD 20771, USA.  
(sandrine.guerlet@lmd.jussieu.fr)

## Abstract

Throughout the Cassini mission, the Cassini Composite InfraRed Spectrometer (CIRS) has acquired thermal infrared spectra in limb viewing geometry that we analyzed to map the temperature and the meridional distribution of five hydrocarbons from the lower to the upper stratosphere (10 mbar – 10 microbar). The exceptional longevity of the Cassini mission enabled us to uniquely investigate the seasonal and temporal changes over almost half a Saturn year to reveal the dynamical and chemical processes that govern Saturn's stratosphere.

In this abstract we review our most important findings: 1) the discovery of an equatorial oscillation in temperature and thermal wind, along with the study of its evolution ; 2) thermal and chemical signatures of the meridional circulation in the middle/upper stratosphere and 3) the detection of benzene and hydrocarbon aerosols in the polar regions, likely produced by ion chemistry in the auroral regions.

## 1. Cassini/CIRS limb observations

The Composite InfraRed Spectrometer (CIRS) recorded spectra of the thermal emission of Saturn's atmosphere in nadir and limb-viewing geometry [1]. We exploited data acquired by Focal Planes 3 and 4 (FP3 and FP4), which covered the spectral range 580-1400  $\text{cm}^{-1}$  with a spectral resolution varying between 0,5 and 15  $\text{cm}^{-1}$ . In limb viewing geometry, the 2x10 detector arrays of FP3 and FP4 were set perpendicular to the limb of the planet, so that each detector probed a different tangent altitude. The projected field of view of one of these detectors was typically 50 to 90km, which is of the order of the atmospheric scale height (~60 km). Hence, the strength of the limb observations was to probe the atmosphere with a much greater vertical coverage and resolution than the nadir-viewing data.

Furthermore, in limb geometry, the long atmospheric path favored the detection and measurement of trace species in the middle stratosphere.

## 2. Data analysis

We employed the forward radiative transfer model coupled to the bayesian inversion method described in [3] to retrieve vertical temperature profiles from the analysis of the  $\nu_4$  methane band (1200-1370  $\text{cm}^{-1}$ ) and of the  $\text{H}_2\text{-H}_2$  and  $\text{H}_2\text{-He}$  collision-induced emission (590-660  $\text{cm}^{-1}$ ). These temperature profiles are constrained between 20 mbar and a few  $\mu\text{bar}$ . Secondly, vertical profiles of the volume mixing ratio of various hydrocarbons can be retrieved from the analysis of their emission bands, such as ethane (centered at 822  $\text{cm}^{-1}$ ) and acetylene (730  $\text{cm}^{-1}$ ).

## 3. Results

In the equatorial regions, we have discovered an Equatorial Oscillation [2,5,9] where the mechanical forcing by upward propagating waves induces temperature anomalies of up to  $\pm 20\text{K}$  in the thermal structure and  $\pm 200$  m/s in the zonal wind field. Our studies show that this oscillation has a temporal period of about 15 terrestrial years (half a Saturn year) and resembles the terrestrial Quasi Biennial Oscillation (QBO) that affects Earth's stratosphere. Outside the equatorial regions, our survey of the thermal structure [3,10] reveals that the seasonal warming and cooling trends observed by CIRS are, to first order, consistent with the predictions from a radiative equilibrium climate model [6]. One notable exception is that the region under the ring's shadow is found warmer than expected from the radiative model, both in 2005 and 2015.

We also studied the spatial distribution of hydrocarbons, by-products of the methane photochemistry, which also undergo significant seasonal change in the upper stratosphere [3,4,10] In

2005, a local maximum of hydrocarbons was observed at 20°-30°N, at odds with the low photochemical production in this region (under the ring's shadow at that time). Together with the high temperature anomaly, we had interpreted this result as the signature of a downwelling branch of the meridional circulation. In 2015, not only has this local maximum vanished, but a new maximum was building in the opposite hemisphere, at 15°-25°S. We suggest that the hydrocarbon and temperature anomalies observed in 2015 in Saturn's upper stratosphere reflects the reversal of a seasonal circulation cell.

Finally, in the we detected stratospheric benzene and hydrocarbon aerosol signatures in both polar regions [7,8]. The amount of benzene and its vertical profile are clearly at odds with predictions from neutral photochemical models and strongly suggest production by ion chemistry. The spectral signatures of Saturn's polar aerosols most strikingly mimic the signatures of Titan's stratospheric aerosols [11]. We assigned the detected vibration modes to aromatic and aliphatic hydrocarbons. The aerosol mass loading was estimated to lie in the range  $1-4 \times 10^{-5} \text{ g cm}^{-2}$ , an order of magnitude less than on Jupiter, which is consistent with the order of magnitude weaker auroral power at Saturn. Nevertheless, we demonstrated that the radiative effects of aerosols is important in the polar regions and could at least partly explain the large seasonal temperature variations observed in these regions.

## Acknowledgements

We acknowledge support by CNES and thank the Cassini/CIRS team for all their work over the years.

## References

- [1] Flasar, F.M. et al., Exploring The Saturn System In The Thermal Infrared: The Composite Infrared Spectrometer, Space Science Reviews, 2004.
- [2] Fouchet et al., An equatorial oscillation in Saturn's middle atmosphere, Nature, 2008.
- [3] Guerlet et al., Vertical and meridional distribution of ethane, acetylene and propane in Saturn's stratosphere from CIRS/Cassini limb observations, Icarus, 2009.
- [4] Guerlet et al., Meridional distribution of  $\text{CH}_3\text{C}_2\text{H}$  and  $\text{C}_4\text{H}_2$  in Saturn's stratosphere from CIRS/Cassini limb and nadir observations, Icarus, 2010.
- [5] Guerlet et al., Evolution of the equatorial oscillation in Saturn's stratosphere between 2005 and 2010 from Cassini/CIRS limb data analysis, Geophysical Research Letters, 2011.
- [6] Guerlet et al., Global climate modeling of Saturn's atmosphere. Part I: Evaluation of the radiative transfer model, Icarus, 2014.
- [7] Guerlet et al., Stratospheric benzene and hydrocarbon aerosols detected in Saturn's auroral regions, Astronomy & Astrophysics, 2015.
- [8] Guerlet et al., Stratospheric benzene and hydrocarbon aerosols observed in Saturn's upper atmosphere, EPSC 2017.
- [9] Guerlet et al., Equatorial Oscillation and Planetary Wave Activity in Saturn's Stratosphere Through the Cassini Epoch, Journal of Geophysical Research, 2018.
- [10] Sylvestre et al., Seasonal changes in Saturn's stratosphere inferred from Cassini/CIRS limb observations, Icarus, 2015.
- [11] Vinatier et al., Optical constants of Titan's stratospheric aerosols in the 70-1500  $\text{cm}^{-1}$  spectral range constrained by Cassini/CIRS observations, Icarus, 2012.



# What is the plasma density in the Enceladus plume?

**Frank Crary**

Laboratory for Atmospheric and Space Physics, University of Colorado, Boulder, USA (frank.crary@lasp.colorado.edu)

## Abstract

The *Cassini* spacecraft made 23 flybys of Enceladus, of which 11 passed through the plume above the moon's south pole. Plasma densities measured during those encounters are a key piece of information in understanding the density of gas and dust in the plume, interaction between Enceladus and the magnetosphere of Saturn and Enceladus' role as the main source of plasma in Saturn's magnetosphere.

Unfortunately, despite six types of independent measurements by the Cassini Plasma Spectrometer (CAPS) and the Radio and Plasma Wave Science (RPWS) instruments, there is no clear or consistent picture of what the plasma density within the plume actually is.

The CAPS electron spectrometer only observed a fraction of the ambient electrons when the spacecraft is charged negatively, as was the case during the Enceladus encounters. It did, however, detect negative ions on at least one encounter, but not on others. To avoid time aliasing, the CAPS instrument did not actuate during the Enceladus encounters, providing 2 and 4 second time resolution, as opposed to ~200 second resolution, but at the expense of only obtaining 2-D cuts through velocity space rather than 3-D coverage. This limits the assumption-independent results to ion flux rather than density.

The RPWS instrument provided three relevant measurements. Close to, but not within, the Enceladus plume, emission at the upper hybrid resonance were used to determine the electron density. However, within the plume itself, impacts from dust particles produced enough "shot noise" to preclude these measurements. Surprisingly, impacts on the RPWS antennas themselves did produce an oscillation in the instruments' wide band data, which has been interpreted as an oscillation at the local plasma frequency. When available, this produces an additional measurement of electron density. Finally, the RPWS instrument's Langmuir probe provided current-voltage curves, which can be fit to determine

ion and electron densities. However, the measured current also depends on the density of charged dust, the density of negative ions, the secondary electron current from energetic particles, and a number of other parameters. As a result, the fits to these data are non-unique and the derived ion and electron densities have high correlated uncertainties.

While all these measurements are in partial agreement at some times, the overall agreement is poor. In many cases, the different techniques give results which disagree by an order of magnitude. In this presentation, I will present the various published results, describe the strengths and weaknesses of each technique, and attempt to reconcile these measurements.

## The geological history of Saturn's icy moons and their interaction with the rings as revealed by the Cassini Radar

A. Le Gall (1), R. West (2), L.E. Bonnefoy (1,3), C. Leyrat (3), M.A. Janssen (2), E. Lellouch (3), R. Sultana (1), and the Cassini RADAR team

(1) Laboratoire Atmosphères, Milieux, Observations Spatiales (LATMOS), Université de Versailles Saint-Quentin (UVSQ) Paris, France ([alice.legall@latmos.ipsl.fr](mailto:alice.legall@latmos.ipsl.fr)), (2) Jet Propulsion Laboratory (JPL), Caltech, CA, USA, (3) Laboratoire d'Etudes Spatiales et d'Instrumentation en Astrophysique (LESIA), Observatoire de Paris-Meudon.

While it was initially designed to examine the surface of Titan through the veil of its optically-opaque atmosphere, the Cassini Radar was occasionally used to observe airless Saturn's icy moons, generally from long ranges. In this paper, we give an overview of the Cassini radar and radiometry distant observations of Mimas, Enceladus, Tethys, Dione, Rhea, Iapetus and Phoebe and describe what they have taught us about the geological history of these objects and their interaction with Saturn and its rings.

### 1. Introduction

For more than 13 years, the Cassini spacecraft has explored the Saturnian system and revealed the wealth of Saturn's moons providing dramatic images of their surfaces. The mission, which ended less than a year ago, has revolutionized our understanding of these icy objects and taught us that they cannot be regarded as frozen worlds anymore (e.g., [1,2]).

However, the collective formation of these moons and subsequent evolution remains an outstanding problem. All of them are composed largely of water ice [3] but their respective history and near environment have led to different regolith composition and structure.

Microwave observations can provide unique insights into the endogenic and exogenic processes that have affected Saturn's moons by putting constraints on the thermal, physical and compositional properties of their subsurfaces. In particular, the Cassini radar, by operating at a wavelength of 2.2 cm [4,5], has expanded the observation of the Saturnian icy satellites to a new and revealing length scale, complementary to that probed by the Cassini's Composite Infrared Spectrometer (CIRS) instrument and ground-based radar systems such as the 12.6-cm wavelength Arecibo observatory.

### 2. Cassini radar and radiometry distant observations of icy moons

Typical distant Cassini radar observations of Saturn's moons occur at ranges between 50,000 km and 500,000 km where the antenna beamwidth is comparable to or greater than the apparent angular extent of the target's disk. These experiments were designed largely for disk-integrated albedo (measured in the instrument active mode) and average brightness temperature albedo (measured in passive mode) calculation.

Ostro et al. (2006, 2010) [6,7] report on the distant observations of Saturn's major airless satellites measured at the beginning of the mission. Since then the observational database has significantly increased to a number of 80 active radar distant observations and 40 distant radiometry observations.

Though unresolved, Cassini distant radar and radiometry observations have revealed intra- and inter-satellites variabilities which bring clues on what is common and what is specific to the history of each of Saturn's airless icy satellites.

### 3. Results

The near-surface emissivity, and the microwave albedo, of Saturn's moons are primarily controlled by the degree of purity of the water-ice regolith [6,7].

At first order, the satellite-to-satellite variabilities and the hemispheric dichotomies shown in Fig. 1 thus reflect subsurface contamination variations resulting from the competition between several effects, including (i) the coating effect of the E-ring (by clean ice) (ii) the coating effect of the vast debris ring from Phoebe (by non-ice compounds) (iii) the geological history of the satellite; and (iv) the efficiency of space weathering at its position within Saturn's magnetosphere.



For instance, around Enceladus, the E-ring guarantees the deposition at the surface of extremely clean water ice that may also be structurally complex and thus very favorable to volume scattering. The decrease in radar brightness and concurrent increase in emissivity from Enceladus outward would then be due to the outward decrease in E-ring flux [8] and hence the endowment of the satellite surface with less ultra-clean ice.

In this paper, we will examine the microwave signature of each Saturnian moon at 2.2 cm as a testimony of its individual evolution. When possible, these observations will be analyzed in light of observations at other wavelengths or by comparison with radio observations of other icy objects. Our overarching goal is to investigate the age and evolution of Saturn's system which is still a much-debated subject (e.g., [9]).

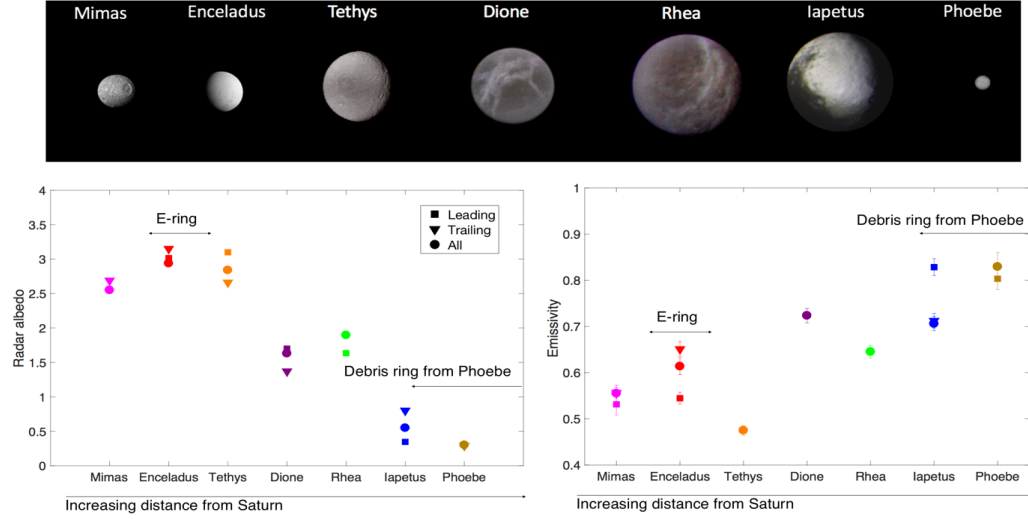


**Figure 1:** Radar albedo and emissivity of Mimas, Enceladus, Tethys, Dione, Rhea, Iapetus and Phoebe derived from Cassini radar and radiometry unresolved observations at 2.2-cm wavelength. The emissivities were estimated dividing the measured disk-integrated brightness temperatures by an equilibrium temperature as described in [5]. For each satellite, when available, values are shown separately for the leading and trailing sides. The locations of the E-ring and the vast debris ring from Phoebe are indicated.

## Acknowledgements

The authors wish to thank the Cassini-Huygens (NASA/ESA/ASI) team for the design, development, and operation of the mission. This project is supported by CNES.

## References

- [1] Porco et al. 2006, *Science* 311, 1393-1401
- [2] Kirchoff and Schenk, 2015, *Icarus* 256, 78–89.
- [3] Clark et al., 1986, In *Satellites*, Univ. of Arizona Press
- [4] Elachi et al., 2004, *Space Sci. Rev.* 115, 71–110.
- [5] Janssen et al. (2009), *Icarus* 200, 222-239.
- [6] Ostro et al., 2006, *Icarus* 183 (2), 479–490.
- [7] Ostro et al 2010, *Icarus* 206, 498-506.
- [8] Verbiscer et al., 2009, *Nature* 461, 1098
- [9] J. Cuzzi, 2018, LPSC #2083

# On the Characteristics of Charged Dust in Saturn's Equatorial Ionosphere – Implications from Cassini RPWS/LP data

**J.-E. Wahlund** (1), E. Vigren (1), M. W. Morooka (1), L. Z. Hadid (1), W. M. Farrell (2), A. M. Persoon (3), W. S. Kurth (3), D. A. Gurnett (3), D. G. Mitchell (4), M. E. Perry (4), J. H. Waite Jr. (5), L. Moore (6), T. E. Cravens (7), M. Galand (8) and A. F. Nagy (9)

(1) Swedish Institute of Space Physics, Box 537, SE-751 21 Uppsala, Sweden (jwe@irfu.se)

(2) NASA/Goddard Space Flight Center, Greenbelt, Maryland, USA

(3) University of Iowa, Iowa City, Iowa, USA

(4) John Hopkins University Applied Physics Laboratory, Laurel, Maryland, USA

(5) Southwest Research Institute, San Antonio, Texas, USA

(6) Center for Space Physics, Boston University, Boston, Massachusetts, USA

(7) Department of Physics and Astronomy, University of Kansas, Lawrence, Kansas, USA

(8) Department of Physics, Imperial College London, London, UK

(9) Department of Atmospheric, Oceanic and Space Sciences, University of Michigan, Ann Arbor, Michigan, USA

## Abstract

The Cassini spacecraft observations close to Saturn have revealed that 1-100 nm-sized dust grains precipitate from the D-ring into the atmosphere. RPWS Langmuir probe ion number density measurements suggest that the charged dust has a profound effect on the ionospheric structure, enhancing the ion number density well above photochemical equilibrium levels, while the electrons tend to become attached to the dust population. We present model calculations of Saturn's equatorial ionosphere and include the effect of charged dust grains that break down into smaller grains/clusters deeper in the atmosphere at an altitude near the ionospheric peak. The model is constrained as far as possible by input from Cassini INMS, RPWS and INCA/CHEMS measurements, and then compared with observed electron and ion number densities by RPWS. From these dust-ionosphere model calculations it is clear that a layer of small singly negatively-charged sub-nm-sized dust grains can explain the RPWS Langmuir probe measurements.

## 1. Introduction

The Cassini spacecraft in-situ measurements monitored the ring material, Saturn's ionosphere and thermosphere. The Radio and Plasma Wave Science (RPWS) observations of ionospheric electron densities [1-4] are determined to high accuracy with

two independent measurement methods and showed an ionospheric peak electron density of 4000-12000 cm<sup>-3</sup> just above 1500 km altitude. The positively charged ion density was greatly enhanced with  $N_e/N_i$  around 10-20% toward the lowest altitudes. These large ion densities (10<sup>4</sup>-10<sup>5</sup> cm<sup>-3</sup>) were clearly not in agreement with photochemical equilibrium models.

## 2. Dust Ionosphere Model

We compare here the RPWS Langmuir probe (LP) measured electron and ion densities in Saturn's ionosphere with an ionosphere model, calculating the ionization production ( $q$ ) directly from Cassini INMS measurements, using measured electron temperatures for rate constants, and including a dust component, based on MIMI and CDA estimates, that we self consistently charge up according to the surrounding plasma. The results show that a greatly enhanced ion number density can be reproduced with similar amounts as RPWS LP observes. We conclude from the model comparison that the equatorial ionosphere of Saturn can be dominated by sub nm-sized grains/cluster ions, probably similar to those encountered in the Earth's polar mesosphere (Figure 1). Our ionosphere model follows the theory/methods employed by [5-7] and solves a set of coupled continuity equations for the temporal evolution of electrons, ions, singly positive charged grains, and up to 10 charge states of negatively charged grains until equilibrium is reached.

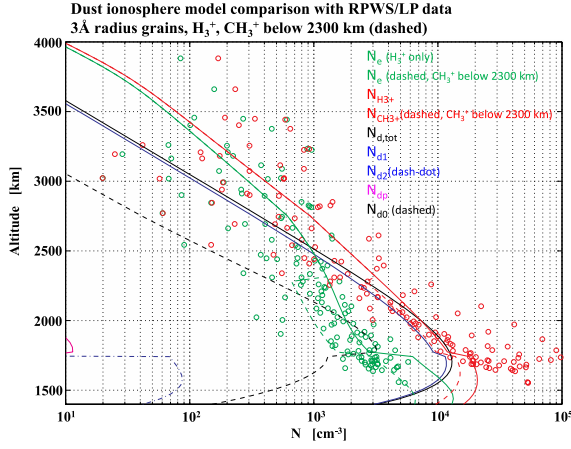


Figure 1: Example model runs with negatively-charged grains of 6 Å size, where  $\text{H}_3^+$  ions are dominant (solid green and red), but  $\text{CH}_3^+$  is also important below an altitude of 2300 km (dashed green and red). The peak total grain number density ( $N_0$ , solid black) is 13,000  $\text{cm}^{-3}$  at 1700 km.

### 3. Summary and Conclusions

We have identified a valid natural explanation for the observed electron and ion number densities by RPWS/LP in Saturn's ionosphere. A "rain" of nm-sized ring-dust deposited in the equatorial region can accumulate a dense layer of sub-nm-sized grains/clusters with a number density of 10,000–15,000  $\text{cm}^{-3}$  near 1700 km altitude. This particulate ring rain is different from that predicted previously by Connerney and Waite (1984), originating instead from the D-ring and its strong interaction with the enveloping, co-rotating ionosphere. The dropout in the electron density by a factor of 10 below 2000 km is also not due to electron loss via the H cycle, but instead it is due to electron attachment to the aerosol congregation in the ionosphere. The impact of the electrons from the H cycle is actually diminished due to this electron loss via this aerosol attachment. Such a dust layer, we show, becomes pre-dominantly singly negatively charged when immersed in the ionospheric plasma, and significantly alters the electron and ion number densities from their photochemical equilibrium values. Electrons will become partly attached to the grains and the relatively stable negatively-charged grain population causes the ion number density to increase, resulting in an  $N_e/N_i$ -ratio to approach 10–20% in the deeper observed parts of Saturn's ionosphere (1500–2000 km altitude above 1-bar level).

### Acknowledgements

The Swedish National Space Board (SNSB) supports the RPWS/LP instrument on board Cassini. L. Z. Hadid is supported by the Swedish Research Council (VR) under contract 2016-05364. W. M. Farrell gratefully acknowledges the Cassini project for internal NASA support. W. S. Kurth and A. M. Persoon are supported by NASA through Contract 1415150 with the Jet Propulsion Laboratory. All Cassini RPWS data are archived in the Planetary Data System (PDS) Planetary Plasma Interaction (PPI) node at <https://pds-ppi.igpp.ucla.edu> on a pre-arranged schedule.

### References

- [1] Wahlund, J.-E., et al. (2017), In situ measurements of Saturn's ionosphere show it is dynamic and interacts with the rings. *Science*, doi:10.1126/science.aao4134.
- [2] Hadid, L. Z., et al. (2018), Saturn's ionosphere: Electron density altitude profiles and D ring electrodynamic interaction from the Cassini grand finale. *Geophys. Res. Lett.*, submitted.
- [3] Morooka, M. W., et al. (2018a), Saturn's ionosphere of dusty heavy ions. *Geophys. Res. Lett.*, submitted.
- [4] Persoon, A. M., et al. (2018), Electron density distributions in Saturn's ionosphere. *Geophys. Res. Lett.*, submitted.
- [5] Draine, B. T., & B. Sutin (1987), Collisional charging of interstellar grains. *Astrophys. J.*, 320, 803–817.
- [6] Meyer-Vernet, N. (2013), On the charge of nanograins in cold environments and Enceladus dust. *Icarus*, 226, 583–590, doi:10.1016/j.icarus.2013.06.014.
- [7] Vigren, E., et al. (2015), On the possibility of significant electron depletion due to nanograin charging in the coma of comet 67P/Churyumov-Gerasimenko near perihelion. *Astrophys. J.*, 798, 130, doi:10.1088/0004-637X/798/2/130.
- [8] Connerney, J. E. P., & J. H. Waite (1984), New model of Saturn's ionosphere with an influx of water from the rings. *Nature*, 312, 136–138, doi:10.1038/312136a0.

# **Titan Trek and IcyMoons Trek: Two New Online NASA Visualization and Analysis Portals for Saturn's Moons**

E. Law (1), B. Day (2)

(1) Jet Propulsion Laboratory, California Institute of Technology. M/S 168-200. 4800 Oak Grove Dr. Pasadena, CA, USA 91109. (Emily.S.Law@jpl.nasa.gov, +01-818-354-6208)

(2) NASA Solar System Exploration Research Virtual Institute. NASA Ames Research Center. M/S 17-1. Moffett Field, CA, USA. 94035. (Brian.H.Day@nasa.gov, +01-650-604-2605)

## **Abstract**

Saturn's moons are the focus of two new online visualization and analysis tools produced by NASA. The Solar System Treks family of online portals provides a suite of interactive visualization and analysis tools. These enable mission planners, lunar scientists, engineers, students, and the general public to access mapped data products from past and current missions for a growing number of planetary bodies. They integrate data from a variety of instruments aboard a number of missions. This presentation will introduce two new portals in the Solar System Trek suite. Titan Trek highlights Saturn's largest moon, and IcyMoons Trek features a number of Saturn's other moons as studied by the Cassini mission.

## **1. Introduction**

This presentation will provide an overview of the uses and capabilities of NASA's Titan Trek and IcyMoons Trek online mapping and modeling portals, new additions to a web-based suite of data visualization and analysis tools designed to support mission planning, scientific research, and education/outreach.

## **2. An Integrated Family of Online Web Portals**

Titan Trek and IcyMoons Trek are two of the newest portals produced and released by NASA's Solar System Treks Project. The project is managed by NASA's Solar System Exploration Research Virtual Institute and developed at NASA's Jet Propulsion Laboratory. These tools enable mission planners, planetary scientists, and engineers to access mapped data products from a wide range of instruments aboard a variety of past and current missions, for a growing number of planetary bodies. Other Solar System Trek portals have been implemented for

bodies including the Moon, Mars, Vesta, and Ceres. Additional portals are in development, including a portal for Mars' moon Phobos.

The Cassini mission conducted multi-instrument investigations of the Saturn system. It sent back a valuable collection of data about those worlds. The Cassini mission commissioned NASA's Solar System Treks Project to implement two new online portals enabling integration, access, and dissemination of data gathered through the mission's investigations of Saturn's moons.

As web-based toolsets, the Titan Trek and Icy Moons Trek portals do not require users to install any software beyond current web browsers. They provide analysis tools that facilitate measurement and study of terrain including distance, height, and depth of surface features. They allow users to easily find and access the geospatial products that are available. Data include imagery from the VIMS and ISS cameras, as well as the RADAR synthetic aperture images, topography, derived physical parameters and community-sourced geological and hydrological mapping products.

Users have the ability to drill down to find the PDS data used to produce the geospatial products. Data products can be viewed in 2D and 3D, and can be stacked and blended together rendering optimal visualization that reveals details that no single data set can show. Data sets can be plotted and compared against each other. In addition to keyboard and mouse control, standard gaming and 3D mouse controllers allow users to maneuver first-person visualizations of flying across the moons' surfaces. The portals also provide users the ability to specify any area of terrain for generation of STL/OBJ files that can be sent to 3D printers to make 3D models. 3D prints and the data visualization capabilities of these portals are particularly valuable in engaging students, educators and general public to personally

explore the moons. In addition to the web portals, standard Application Programmable Interfaces (API) are available to facilitate access and dissemination of the data products to external applications and use.

### **3. Summary and Conclusions**

Investigators of Saturn's moons have powerful new visualization and analysis tools available to them with the release of the new Titan Trek and IcyMoons Trek portals. Individually, these portals enable detailed study of Saturn's moons by researchers, mission planners, educators, students, and the general public. As components of the Solar System Treks Project, with its growing number of planetary bodies represented, these new portals also facilitate comparative planetology studies between and among Saturn's moons, and between these moons and other bodies.

### **Acknowledgements**

The authors would like to thank the Cassini Mission, the Planetary Science Division of NASA's Science Mission Directorate, NASA's SMD Science Engagement and Partnerships, and the Advanced Explorations Systems Program of NASA's Human Exploration Operations Directorate for their support and guidance in the development of Titan Trek and IcyMoons Trek.

# Saturn's upper atmosphere from the Cassini/UVIS Grand Finale stellar occultations

**Tommi T. Koskinen** (1), Zarah L. Brown (1), Robert A. West (2), Alain Jouchoux (3) and Larry W. Esposito (3)

(1) Lunar and Planetary Laboratory, University of Arizona, Arizona, USA, (2) Jet Propulsion Laboratory, California Institute of Technology, California, USA, (3) Laboratory for Atmospheric and Space Physics, University of Colorado, Colorado, USA (tommi@lpl.arizona.edu)

## Abstract

A global picture of Saturn's upper atmosphere is necessary to understand the dynamics, energy balance and minor species composition in the thermosphere. Occultation data from Voyager/UVS and Cassini/UVIS have been used to study this poorly known region of the atmosphere. The previous data, however, are largely concentrated at low to mid-latitudes and were obtained sporadically at different times, complicating the separation of temporal and spatial trends. The Grand Finale occultations overcome these limitations as the data were obtained within six weeks in the summer of 2017. Together with the observations from 2016, they provide a vital new look at meridional trends in Saturn's thermosphere. We present temperature and density profiles retrieved from these occultations, including a first look at the polar thermosphere.

## 1. Introduction

Despite recent advances enabled by the Cassini mission, our understanding of Saturn's upper atmosphere is still relatively poor. In particular, the higher than expected temperatures in the thermosphere, that are also observed on Jupiter, Neptune and Uranus, remain a major problem that has evaded a clear solution. The leading mechanisms to explain these temperatures i.e., the dissipation of upward-propagating gravity waves, auroral heating followed by the redistribution of energy to lower latitudes, and low-latitude electrodynamics, depend on atmospheric dynamics [1]. Circulation in the thermosphere, however, is unknown on global scales due to the lack of observations that could constrain it. The density and temperature profiles retrieved from the occultations that we will present probe the thermosphere from low latitudes to the poles (see Figure 1). They provide a snapshot of Saturn's upper atmosphere at the end of the Cassini mission. The results constitute the most extensive observations of a

giant planet upper atmosphere to date. The meridional gradients evident in the data provide the first global constraint on the redistribution of energy and dynamics in the thermosphere.

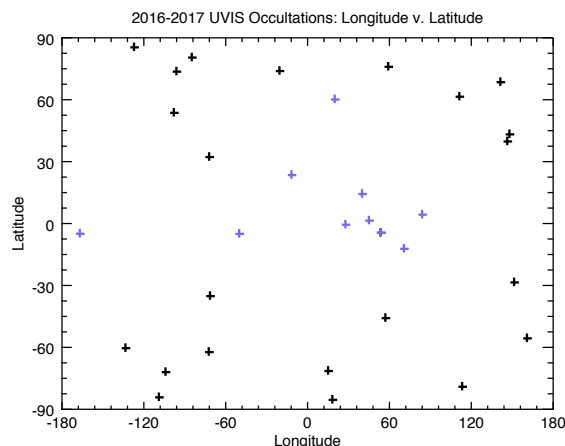


Figure 1: Half-light latitude and longitude of the occultations observed in 2016 (purple) and 2017 (black).

## 2. Methods

We retrieve the  $H_2$  density and temperature in the thermosphere from the 2016–2017 occultations observed in the EUV channel of the Cassini/UVIS instrument [2]. The cross section of  $H_2$  depends on temperature and we use an iterative method to retrieve the density and temperature profiles, assuming hydrostatic equilibrium. Our method accounts for the change in temperature along the line of sight and the oblateness of Saturn's atmosphere. Details of the retrieval and error analysis are given in Koskinen et al.[3].

### 3. Summary and conclusions

Our results constrain the shape of the density levels in the thermosphere and temperature as a function of latitude and height. Superimposed on the expected oblate shape of the atmosphere, we confirm that pressure levels are more extended at high latitudes than at low latitudes, indicative of polar heating. Meridional trends in temperature, however, point to surprising high-latitude features that have not been predicted by previous models. We also find evidence of atmospheric waves in many of the occultations that have implications for the momentum and energy balance of the thermosphere.

### References

- [1] Strobel, D. F., Koskinen, T. T. and Müller-Wodarg, I. C. F.: Saturn's variable thermosphere, arXiv:1610.07669, 2016.
- [2] Esposito, L. W., et al.: The Cassini Ultraviolet Imaging Spectrograph investigation, Space Sci. Rev., Vol. 115, pp. 299-361, 2004.
- [3] Koskinen, T. T., Sandel, B. R., Yelle, R. V., Strobel, D. F., Müller-Wodarg, I. C. F., Erwin, J. T.: Saturn's variable thermosphere from Cassini/UVIS occultations, Icarus, Vol. 260, pp. 174-189, 2015.



# Saturn's equatorial ionosphere: dominance of heavy ions and model comparisons with Cassini Grand Finale data

L. Moore (1), T. E. Cravens (2), I. Müller-Wodarg (3), M. E. Perry (4), J. H. Waite (5), R. Perryman (5), A. Nagy (6), D. Mitchell (4), A. Persoon (7), J.-E. Wahlund (8), M. W. Morooka (8)

(1) Boston University, Center for Space Physics, Massachusetts, USA (moore@bu.edu); (2) Department of Physics and Astronomy, University of Kansas, Lawrence, Kansas, USA; (3) Blackett Laboratory, Imperial College London, Prince Consort Road, London SW7 2AZ, UK; (4) Johns Hopkins University Applied Physics Laboratory, Laurel, Maryland, USA; (5) Southwest Research Institute, San Antonio, Texas, USA; (6) Department of Climate and Space Sciences and Engineering, University of Michigan, Ann Arbor, Michigan, USA; (7) Department of Physics and Astronomy, University of Iowa, Iowa City, Iowa, USA; (8) Swedish Institute of Space Physics, Box 537, SE-751 21 Uppsala, Sweden

## Abstract

The first in situ measurements of Saturn's upper atmosphere were obtained by the Cassini spacecraft from proximal orbits (spanning April – September 2017) during the Grand Finale phase of the 13-year mission. These data find definitive evidence for a strong influence of Saturn's rings on its equatorial upper atmosphere, manifesting as an influx of grains and related material [1-5].

An influx of ring-derived water was expected, as that would act as a quenching agent in Saturn's ionosphere, reducing modeled electron densities to observed values. Water was indeed found, but the bulk of the gaseous species detected appear to be methane and other organics. The first-order impact of these more complex molecules on Saturn's ionosphere is similar to that of water, in that they reduce the modeled electron density by converting long-lived ions to short-lived ions. However, they also significantly complicate the ionospheric chemistry.

Here, we present model comparisons with in situ ion and electron density measurements. While some model-data discrepancies remain, we are able to demonstrate that:

- (1) based on Ion Neutral Mass Spectrometer (INMS) measurements, the light ions ( $H^+$ ,  $H_2^+$ ,  $H_3^+$ , and  $He^+$ ) are broadly consistent with the makeup of the observed neutral species [5-6]; and
- (2) molecular ions dominate Saturn's low altitude equatorial ionosphere, with  $H_3O^+$  playing a major role, even for the reduced levels of water influx [6].

Other important heavy ions are uncertain, but are likely to include  $HCO^+$ ,  $HCO_2^+$ ,  $N_2H^+$ ,  $CH_5^+$ ,  $C_2H_3^+$ , and other hydrocarbon ions [6]. The dominance of such heavy ions is a surprise, as expectations based on previous model-data comparisons were that  $H^+$  and  $H_3^+$  would be the only major ions above the homopause, with  $H_3O^+$  becoming more prominent in regions of enhanced water influx. Future Earth-based observations of some of these ion species may help to track the evolution of Saturn's rings as they lose mass to its atmosphere.

## References

- [1] Waite, J.H., Jr. et al. (2018), INMS Observations of Chemical Interactions between Saturn's Atmosphere and Rings, *Science*, submitted.
- [2] Hsu, H.-W., et al. (2018), Cosmic Dust Analyzer onboard Cassini Collects Material from Saturn's Main Rings, *Science*, submitted.
- [3] Perry, M.E., et al. (2018), Material flux from the rings of Saturn's into its atmosphere, *Geophys. Res. Lett.*, submitted.
- [4] Yelle, R.V., et al. (2018), Thermal Structure and Composition of Saturn's Upper Atmosphere from Cassini/INMS Measurements, *Geophys. Res. Lett.*, submitted.
- [5] Cravens, T.E., et al. (2018), The Ion Composition of Saturn's Equatorial Ionosphere as Observed by Cassini, *Geophys. Res. Lett.*, submitted.
- [6] Moore, L., et al. (2018), Models of Saturn's equatorial ionosphere based on in situ data from Cassini's Grand Finale, *Geophys. Res. Lett.*, submitted.



## Saturn's Atmospheric Photochemistry: Chemistry and Haze in Ring-Shadowed Atmosphere and within the Hexagon

**S.G. Edgington** (1), S.K. Atreya (2), E.H. Wilson (3), K.H. Baines (1,4), R.A. West (1), G.L. Bjoraker (5), L.N. Fletcher (6), T. Momary (1)

(1) Jet Propulsion Laboratory/California Institute of Technology, USA (scott.g.edgington@jpl.nasa.gov), (2) University of Michigan, USA, (3) Space Environment Technologies, USA, (4) University of Wisconsin, USA, (5) NASA Goddard Space Flight Center, USA, (6) University of Oxford, UK

### Abstract

Cassini has orbited Saturn for over thirteen years. During this Saturn half-year, the ring shadow has moved from covering a relatively large portion of the northern hemisphere (Figure 1a) to covering a large swath of territory south of the equator as solstice approaches. At Saturn Orbit Insertion on July 1, 2004, the sub-solar point was  $\sim 24^\circ$  South. At this time, the projection of the optically thick B-ring onto Saturn reached as far as  $40^\circ$ N at the central meridian ( $\sim 52^\circ$ N at the terminator). At its maximum extent, the ring shadow can reach as far as  $48^\circ$ N/S ( $\sim 58^\circ$ N/S at the terminator). The net result is that the intensity of both ultraviolet and visible sunlight penetrating into any particular latitude will vary greatly depending on both Saturn's axis relative to the Sun and the optical thickness of each ring system. In essence, the rings act like semi-transparent Venetian blinds (Figure 2) over the atmosphere of Saturn.

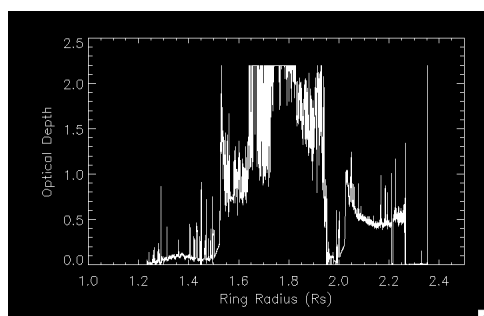


Figure 2. The optical depth of Saturn's rings in the ultraviolet (Josh Colwell, *pers. comm.*) The rings act like a periodic Venetian blind that will shield atmospheric molecules from solar photons.

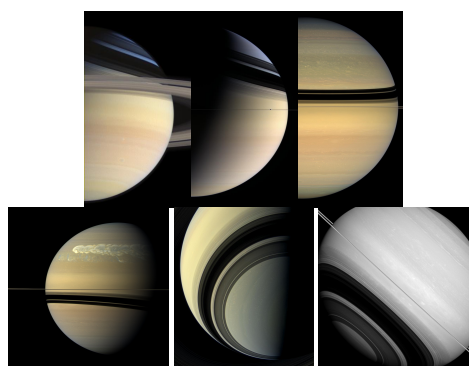


Figure 1. Saturn's atmosphere changes in response to the changing inclination of the ring plane relative to the Sun: (a) December 14, 2004, (b) March 16, 2006, (c) April 23, 2008, (d) July 6, 2011, (e) July 29, 2013, (f) November 24, 2014. Images are courtesy of NASA/JPL/Space Science Institute.

Previous work [1,2] examined the variation of the solar flux as a function of solar inclination, i.e.  $\sim 7.25$  year season (Figure 3) at Saturn. Beginning with methane, phosphine and ammonia, we investigate the impact on production and loss rates of the long-lived photochemical products leading to haze formation at several latitudes over a Saturn year. Here, we report on how the oscillating ring shadow modifies the photolysis and production rates of hydrocarbons in Saturn's stratosphere and upper troposphere, including acetylene, ethane, and propane. The magnitude of reflected UV sunlight from the rings on the atmosphere illuminated by ringshine is also explored in this work. Similarly, we assess the impact of these effects on phosphine abundance, a disequilibrium species whose presence in the upper troposphere is a tracer of convection processes in the deep atmosphere. Comparison to the corresponding rates for the clear atmosphere and for the case of

Jupiter, where the solar insolation is known to be insignificant ( $\sim 3^\circ$  inclination), will also be presented. Our ongoing analysis of Cassini's CIRS, UVIS, and VIMS datasets that provide abundances of key molecules and estimates of the evolving haze content of the both hemispheres is updated.

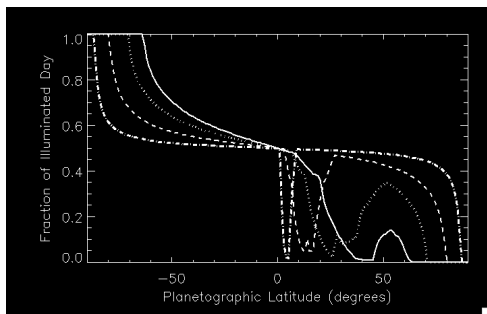


Figure 3. This plot illustrates the fraction of Saturn's day that is illuminated by the Sun as a function of solar declination, i.e. season. The curves correspond to sub-solar points of  $26.7^\circ\text{S}$  (solid),  $19.6^\circ\text{S}$  (dotted),  $10.7^\circ\text{S}$  (dashed), and  $3.5^\circ\text{S}$  (dot-dashed). Ultimately, this will determine the flux of photons allowed to enter the atmosphere relative to those of a clear, unshaded atmosphere.

The implications for dynamical mixing on the transport of molecules and haze is explored. In particular, we will examine how the now famous hexagonal jet stream (Figure 4) acts like a barrier to transport, isolating Saturn's north polar region from outside transport of photochemically-generated molecules and haze. Future research will explore the role to which increasingly intense sunlight plays in the buildup of hydrocarbon hazes in the polar region and determine exactly how isolated polar region is unaffected by transport from more southerly latitudes.

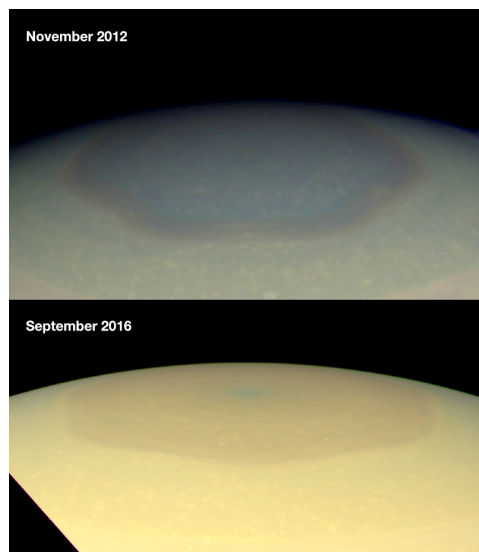


Figure 4. One of the aims of this exercise is to characterize the haze content Saturn's atmosphere. Several Cassini data sets from ISS (above) and VIMS (below) are being used to meet this goal.

## Acknowledgements

The research described in this paper was carried out in part at the Jet Propulsion Laboratory, California Institute of Technology, under a contract with the National Aeronautics and Space Administration. Copyright 2017, California Institute of Technology. Government sponsorship is acknowledged.

## References

- [1] Edgington, S.G., A.A. Simon-Miller, R. Achterberg, G. Bjoraker, P. Romani, F.M. Flasar, J. Colwell, 2006. Adaptation of a 2-D Photochemical Model to Improve Our Understanding of Saturn's Atmosphere. *Bull. American Astron. Soc.*, **38**, 499 (#11.23).
- [2] Edgington, S.G., R.A. West, K.H. Baines, S.K. Atreya, E.H. Wilson, G.L. Bjoraker, L.N. Fletcher, and T. Momary, 2012. Photochemistry in Saturn's Ring Shadowed Atmosphere: Modeling, Observations, and Preliminary Analysis. *Bull. American Astron. Soc.*, **38**, 499 (#11.23).

# A clue about Saturn's normal modes from analysis of Cassini's Grand Finale gravity orbits

D. Durante, P. Racioppa, and L. Iess

Sapienza University of Rome, Department of Mechanical and Aerospace Engineering, Rome, Italy  
(daniele.durante@uniroma1.it)

## Abstract

After more than 13 years spent orbiting about Saturn, the Cassini spacecraft ended its mission on September 15, 2017 with a deliberate plunge into Saturn's atmosphere. In its final phase, the Grand Finale, Cassini provided the most detailed insights on Saturn's rings, atmosphere, and interior. Out of the 22 proximal orbits, six pericenter passes have been devoted to the determination of the gravity field of the planet. Previous determination was carried out by studying the motion of the satellites. Current observations are far more accurate for determining Saturn's gravity field since the spacecraft passes very close to the cloud tops. In addition, the first gravitational measurement of the rings' masses has been made.

During each of the six passes, Cassini was tracked for about 24 hours by the antennas of both NASA's Deep Space Network and ESA's ESTRACK network, providing high quality Doppler measurements at X-band. The RMS noise level is as low as 0.02 mm/sec, at 30 s integration time, which, together with the favorable orbital geometry, allow a good determination of Saturn's gravity field.

The analysis of the Doppler data is complicated by an unexpected non-zonal and/or non-static component of the gravity field. In fact, for a rotating fluid planet in hydrostatic equilibrium, only zonal gravity coefficients are expected. Non-zonal components may arise from different mechanisms. One of the possible explanations is to suppose a time-varying gravity field, related to Saturn's normal modes. The presence of normal modes inside Saturn has already been proved with ring seismology [1, 2], and used to constrain the interior structure of the planet [3].

In general, the inclusion of normal modes in the analysis of the Doppler data allow us to obtain a satisfactory solution. However, the discrimination of the relevant modes is almost impossible due to the limited temporal coverage. The data analysis has shown that different combinations of gravity and/or acoustic modes can be employed to obtain a good fit of the residuals, and many more combinations are surely possible. We report on the analysis of the gravity data by means of several subsets of normal modes to explain the non-zonal component of Saturn's gravity field.

## Acknowledgements

This research was carried out under the sponsorship of the Italian Space Agency.

## References

- [1] Hedman, M. M. and P. D. Nicholson (2013). *Kronoseismology: Using Density Waves in Saturn's C Ring to Probe the Planet's Interior*, The Astronomical Journal 146, 12.
- [2] Hedman, M. M. and P. D. Nicholson (2014). *More Kronoseismology with Saturn's rings*, Monthly Notices of the Royal Astronomical Society 444, 1369–1388.
- [3] Fuller, J. (2014). *Saturn ring seismology: Evidence for stable stratification in the deep interior of Saturn*, Icarus 242, 283–296.

## **Ring- and Moon-Associated Energetic Particle dropouts observed by MIMI-LEMMS during Cassini's Ring-Grazing Orbits**

**Geraint H. Jones** (1,2), E. Roussos (3), P. Kollmann (4), N. Krupp (3), D. Mitchell (4)

(1) Mullard Space Science Laboratory, University College London, UK, (2) The Centre for Planetary Sciences at UCL/Birkbeck, London, UK, (3) Max Planck Institute for Solar System Research, Goettingen, Germany, (4) Johns Hopkins University Applied Physics Laboratory, Laurel, MD, USA (g.h.jones@ucl.ac.uk)

### **Abstract**

During December 2016-April 2017, the Cassini spacecraft performed 19 orbits with periapses just outside Saturn's main rings. These ring plane crossings allowed magnetic field lines threading the outer regions of the main ring system to be sampled close to the equatorial plane. Trapped energetic particles have been previously shown to provide valuable information on the presence of moons, rings, and incomplete ring arcs that complements the data provided by remote sensing instruments. We report on observations of this region by the LEMMS sensor of Cassini's Magnetospheric Imaging System, MIMI. We concentrate on results relevant to the region surrounding the moons Janus and Epimetheus at 2.4 to 2.8 Saturn radii from the planet's centre. We present the inferences that can be drawn about this region from absorption signatures due to those moons plus the ring material that orbits near to them, slightly complicated by the northward offset of Saturn's magnetic equator.

### **Acknowledgements**

Work by GHJ is partially supported by the UK Science and Technology Facilities Council.

## Survey of Saturn's magnetosheath and its boundaries throughout the Cassini mission

**Jackman, Caitriona** (1), Thomsen, Michelle (2) Sergis, Nick (3) and Dougherty, Michele (4)

(1) Department of Physics and Astronomy, University of Southampton, Southampton, SO17 1BJ, UK, (2) Planetary Science Institute, 1700 East Fort Lowell, Suite 106, Tucson, AZ, 85719, USA, (3) Office of Space Research and Technology, Academy of Athens, Athens, Greece (4) Blackett Laboratory, Imperial College London, London, UK.

(c.jackman@soton.ac.uk)

### Abstract

The Cassini spacecraft orbited the planet Saturn from July 2004 – September 2017, and its varied orbital trajectory took it across the magnetopause and bow shock boundaries multiple times, at varying radial distances, local times, latitudes, and phases of the solar cycle. Here we present a complete list of these boundary crossings, derived primarily using data from the Cassini magnetometer instrument. In this work, we use the list to select intervals when Cassini spent time in Saturn's magnetosheath and in the upstream solar wind. We statistically examine these intervals over the full solar cycle of Cassini's exploration and examine local time asymmetries in the sheath, as well as the processing of the interplanetary magnetic field from the solar wind through the bow shock to the magnetopause, quantifying the impact of features such as Saturn's polar flattening on the magnetosheath properties. Furthermore, we combine this list with a recently published dataset of magnetosheath parameters to establish the link between the magnetosheath parameters and the upstream solar wind dynamic pressure, which allows us to explore the response of the

magnetosphere to solar wind dynamic pressure variations.

### References

Thomsen, M. F., Coates, A. J., Jackman, C. M., Sergis, N., Jia, X., & Hansen, K. C. (2018). Survey of magnetosheath plasma properties at Saturn and inference of upstream flow conditions. *Journal of Geophysical Research: Space Physics*, 123. <https://doi.org/10.1002/2018JA025214>

# Titan's interior structure after Cassini/Huygens

**Christophe Sotin** (1), Nicolas Rambaux (2), Ondrej Cadek (3), Klara Kalousova (3), Adrien Neri (4) and Bruno Reynard (4)  
 (1) Jet Propulsion Laboratory–California Institute of Technology, Pasadena, CA, USA, (2) IMCCE, Observatoire de Paris – PSL Research University, Sorbonne Université, 77 Avenue Denfert-Rochereau, 75014 Paris, France, (3) Charles University, Faculty of Mathematics and Physics, Department of Geophysics, V Holešovickách 2, 180 00 Praha 8, Czech Republic, (4) Laboratoire de Géologie de Lyon: Terre, Planète, Environnement, Campus de la Doua, 2 rue Raphaël Dubois, 69622 Villeurbanne Cedex, France ([christophe.sotin@jpl.nasa.gov](mailto:christophe.sotin@jpl.nasa.gov))

## Abstract

Several data sets acquired by the Cassini-Huygens mission are combined with petrological models of hydrated silicates and numerical simulations of heat transfer through the different layers to provide a model of Titan's interior structure. The gravity data are interpreted for different models of mass distribution to explain the topography. The preferred model has a moment of inertia 3% smaller than that predicted by the Radau-Darwin equation. This study suggests that Titan's moment of inertia is 3% smaller than predicted by the Radau-Darwin equation. The interior structure would be composed of an inner silicate core of 1885 km overlaid by a 690 km thick hydrosphere composed of a convective high-pressure ice layer, a salty ocean, and a convective icy crust that includes a thin outer layer made of ethane-clathrates at the poles.

## 1. Introduction

Titan is the only large icy moon with a dense atmosphere, organic molecules, and liquid reservoirs at the surface. The Cassini mission has revealed Titan as being a complex world with a methane cycle that requires exchange processes between the interior and the atmosphere. It is also an ocean world with the presence of a salty water ocean below an icy crust [1]. The combined analysis of gravity and topography data can help constrain its interior structure and dynamics (section 2). Implications for the size and density of the silicate core are then described in section 3 before describing the different layers of the hydrosphere in section 4 and the potential for transport of surface organics to the ocean and the transport of salts and volatiles from the deep interior to the surface.

## 2. Interior models

Titan's shape has been measured by radar altimetry, synthetic-aperture radar topography and stereo radargrammetry [1]. It is turned into a topographic map by subtracting an ellipsoid that contains the rotational and tidal potentials. The difference between this ellipsoid and an equipotential surface calculated with the gravity coefficients up to degree 4 [3] is less than 25 m. The data are inverted into a spherical harmonics model up to degree 8 (Fig. 1). The inversion puts more weight on the altimetry data which have a better precision. The topographic map shows a strong degree (2,0) corresponding to the polar depressions, but no obvious equatorial degree (2,2).

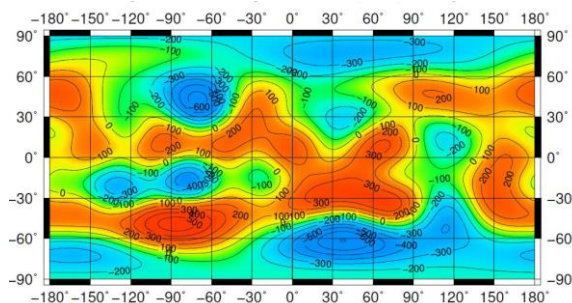


Figure 1: Titan's topography obtained from the spherical harmonics decomposition up to degree 8.

The interior model consists of four nested shells characterized by their density and outer and inner radius: icy crust, ocean, high-pressure ice layer, and silicate core. The position of each interface is calculated by solving the Clairaut equations. The ratio of  $J_2$  to  $C_{2,2}$  is close to 10/3, suggesting hydrostatic equilibrium. However, surface topography generates mass anomalies at the surface whose influence on the values of the degree 2 gravity coefficients can be large [4]. We assess the effect of topography by using a 3D spherical code where



lateral mass anomalies can be included at each of the four interfaces. The effect of topography at the pole is investigated for both Airy and Pratt models based on geodynamical processes [5, 6, 7]. We also investigate the effect of non-compensated equatorial topography.

Results are summarized in Fig. 2 for the  $J_2$  gravity coefficient. The nominal model assumes that both the polar depressions and the equatorial topography are compensated. For 100% compensation of the equatorial topography the Pratt model and the Airy model explaining the polar depressions provide slightly different values of  $J_2$  because the Airy model is compensated at the icy crust / ocean interface whereas the Pratt model is compensated within a few kilometres below the surface. The value of  $J_2$  decreases very rapidly with decreasing degree of compensation. On the other hand, a non-compensated equatorial topography (red points and curves) increases the value of  $J_2$  suggesting that non-compensated polar topography could be hidden by non-compensated equatorial topography. Another possibility would be to have a smaller value of the moment of inertia (smaller value of  $J_2$ ). The parameter space of interior models is large but however bounded as we cannot change these three parameters independently from each other. In addition, the value of  $C_{2,2}$ , not shown here, provides additional constraints.

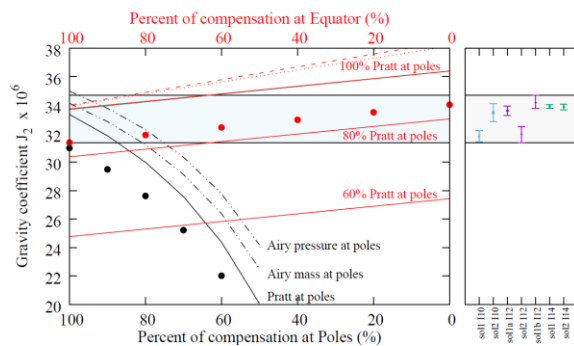


Figure 2: Value of the  $J_2$  gravity coefficient for different degrees of compensation at the pole and at the equator. The right panel shows the values of  $J_2$  inferred from different inversions [2, 3].

### 3. Implications for the composition of the silicate core

The nominal isostatic model leads to a large silicate core with a low density that corresponds to that of Mg-antigorite. It would imply that there is no iron in the silicate core. This seems difficult to accept. So a model with a smaller and denser core (smaller value of  $J_2$ ) is appealing. This is possible with a non-compensated equatorial topography which leads to a silicate core 125 km smaller and 270 kg/m<sup>3</sup> denser leading to a Fe# much closer that that of carbonaceous chondrites.

## 4. Structure of the hydrosphere

The present structure is very simple with constant density for each layer. Ongoing work is investigating the effect of more realistic equations of state (EoS) on the value of the MoI. With the present model, the thicknesses of the icy crust, ocean, and HP ice layer are 75, 250, and 365 km, respectively. The HP-ice would be convecting in a regime that allows for the transfer of volatiles from the silicate core to the ocean [8].

## 5. Summary and Conclusions

Now that the Cassini mission ended, it is possible to use the available data sets to infer the most probable interior structure. However, major questions remain such as the size of the silicate core, the thickness of the HP ice layer, and the dynamics of the icy crust. Future landed missions equipped with seismometers and orbiter missions acquiring more precise topography and gravity fields would provide the missing data to understand the interior structure and dynamics of this complex organic world.

## Acknowledgements

This work has been performed at the Jet Propulsion Laboratory, California Institute of Technology, under contract to NASA.

## References

- [1] P. Corlies et al. (2018) GRL, 44, 11,754-11,761.
- [2] Iess L. et al. (2010) Science, 327, 1367.
- [3] Iess L. et al. (2012) Science 337, 457.
- [4] P. Gao and D.J. Stevenson (2013) Icarus, 226, 1185–1191.
- [5] F. Nimmo and B.G. Bills (2010) Icarus 208, 896–904
- [6] J. Kverka et al. (2018) Icarus, in revision
- [7] Choukroun M. and Sotin C. (2012) GRL, 39, L04201.
- [8] Kalousova K. et al. (2018) Icarus, 299, 133-147.